Visible-Light-Induced Chlorine Photoelimination from Acridinium-Phosphine Gold(III) Complexes

Shantabh Bedajna[a], Kristopher G. Reynolds[b], Mohammadjavad Karimi[a], Elishua D. Litle[a], Daniel G. Nocera[b*], and François P. Gabbaï[a*]

[a]Texas A&M University, Department of Chemistry, College Station, TX 77843, United States

[b]Harvard University, Department of Chemistry and Chemical Biology, Cambridge, MA 02138, United States

Emails: francois@tamu.edu, dnocera@fas.harvard.edu

Supporting Information

Table of Contents

1 Experimental details S2
1.1 General considerations S2
1.2 Synthesis S2
2 NMR spectra S4
3 UV-vis spectroscopy S9
4 Photolysis studies S11
5 Quantum yield measurements S14
6 Transient Spectroscopy S16
6.1. General considerations for Nanosecond TA Spectroscopy (nsTA) S16
6.2. General considerations for Femtosecond TA Spectroscopy (fsTA) S16
6.3. Transient Spectroscopy Data S18
6.3.2. TA on [1a][BF_4] S18
6.5. UV-visible absorption spectroscopy S19
7 Catalysis Study S20
8 Computational studies S21
8.1 General methods S21
8.2 Simulated UV-vis spectra S22
8.3 TD-DFT studies and relevant Kohn-Sham orbitals S23
8.4 Optimized geometries S25
8.5 Cartesian coordinates of the geometry optimized structures S28
9 X-ray diffraction analysis S33
9.1 Experimental details S33
9.2 CCDC deposition numbers S33
10 References S33

1 Experimental details

1.1 General considerations

All reactions and manipulations were carried out under an atmosphere of dry, O_2-free nitrogen using standard Schlenk techniques, unless stated otherwise. A nitrogen-filled glove box was used to manipulate the solids, store air-sensitive materials, carry out room temperature reactions, recover reaction products, and prepare samples for analysis. Solvents were dried by refluxing under N_2 over Na/K (Et_2O and THF), Na (Hexanes) or CaH_2 (MeCN and CH_2Cl_2), and stored under a nitrogen atmosphere over 3Å molecular sieves. The deuterated solvents (CD_2Cl_2, $CDCl_3$, CD_3CN) used in this work were distilled over CaH_2 and stored over molecular sieves before use. Chemicals were purchased from commercial suppliers and used as received. ^1H, ^{13}C, ^{19}F and ^{31}P NMR spectra were recorded on a Bruker Avance II 400, a Bruker Avance 500, or a Bruker Avance 500 cryoprobe. ^1H and ^{13}C chemical shifts are expressed as parts per million (ppm, δ) downfield of tetramethylsilane (TMS) and are referenced to $CDCl_3$ (7.26/77.16 ppm) or CD_2Cl_2 (5.32/53.84 ppm) residual solvent peaks. ^{31}P NMR spectra were referenced to H_3PO_4. Mass spectrometric analyses were performed in-house at the Texas A&M Chemistry Mass Spectrometry Facility using a Thermo Scientific Q Exactive Focus instrument. Elemental analyses were performed at Atlantic Microlab (Norcross, GA). The starting material [**1a**][BF_4] was synthesized according to the literature with spectral analyses being consistent with previously established values.[1]

1.2 Synthesis

Synthesis of [**2a**][BF_4]

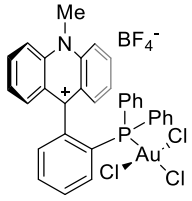

[**1a**][BF_4] (50 mg, 0.064 mmol) was dissolved in acetonitrile (2 mL) in a 20 mL scintillation vial wrapped in aluminum foil. $PhICl_2$ (45 mg, 0.161 mmol) was added, and the solution was stirred for 30 minutes in the dark. A 10 mL portion of Et_2O was then added to precipitate a pale yellow powder. The solid residue was then filtered and washed with hexane (3 x 5 mL) and Et_2O (3 x 5 mL) to afford 40.0 mg of [**2a**][BF_4] (yield: 73%). Yellow block shaped single crystals were obtained by layering Et_2O on a CH_3CN solution of the compound. **^{1}H NMR** (500 MHz, CD_3CN) δ 8.42 (m, 3H), 8.31 (t, *J* = 8.4 Hz, 2H), 8.05 (m, 2H), 7.88 (d, *J* = 9.3 Hz, 2H), 7.75 (t, *J* = 7.47 Hz, 2H), 7.49-7.45 (m, 3H), 7.30-7.25 (m, 4H), 7.12 (m, 4H), 4.68 (s, 3H, NMe) **^{13}C{^{1}H} NMR** (126 MHz, CD_3CN) δ 157.3 (s),140.2 (d, J=13.28 Hz), 139.9, 138.3 (d, J=7.1 Hz), 136.6 (d, J=11.3 Hz), 134.5, 133.1 (d, *J* = 9.0 Hz), 130.82 (d, *J* = 13.6 Hz), 130.6, 129.2, 129.0, 129.0, 127.1, 124.5, 124.0, 122.0, 121.4, 119.1, 39.4. **^{31}P{^{1}H} NMR** (162 MHz, CD_2Cl_2, 298 K) δ: 42.6 **Elemental Analysis** calc'd for $C_{32}H_{25}AuBCl_3F_4NP$: C: 45.50; H: 2.98. found: C: 45.13; H: 3.11.

Synthesis of the ligand precursor **L**

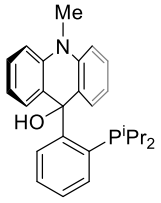

2-bromophenyldiisopropyl phosphine (748 mg, 2.2 mmol) was dissolved in 20 mL dry THF and cooled to -78 °C. A solution of *n*BuLi (2.5 M in hexanes, 1.0 mL, 2.6 mmol) was added dropwise, resulting in a deep orange solution, which was stirred at the same temperature for 1 hour. A suspension of N-methyl acridone (543 mg, 2.6 mmol) in THF (10mL) was then transferred by a cannula into the reaction mixture at -78 °C. The resulting mixture was stirred for 1 h, then warmed to ambient temperature and further stirred for 18 h. The reaction was quenched by adding a saturated aqueous ammonium chloride solution, and the aqueous phase was extracted with Et_2O (3 × 20 mL). The combined organic fractions were dried over $MgSO_4$ and the volatiles were removed *in vacuo*. The dark red residue was triturated with hexanes, giving a brown powdery solid. Washing the residue with a minimum amount of acetonitrile and drying *in vacuo* gave the crude product as a beige solid, which was used in the next reaction without further purification. The product was stored in a N_2 filled glove box. **^{1}H{^{1}H} NMR** (500 MHz, CD_3CN) δ 8.31 (s, 1H), 7.46 (m, 2H), 7.33 – 7.26 (m, 2H), 7.21 (m, 2H), 7.06 (d, *J* = 8.40, 2H), 6.87 (d, *J* = 7.72, 2H), 6.71 (t, *J* = 7.97, 2H), 3.62 (s, 3H), 1.50 (m, 2H), 0.80 – 0.69 (m, 6H), 0.10 (m, 6H). **^{31}P{^{1}H}** (162 MHz, CD_3CN) δ -5.8.

Synthesis of [**1b**][OTf]

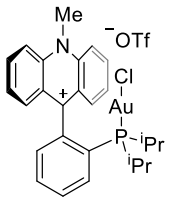

L (50 mg, 0.12 mmol) was dissolved in CH_2Cl_2 (4 mL) in a 20 mL scintillation vial under nitrogen. (tht)AuCl (40mg, 0.12 mmol) was added, and the solution was stirred for 15 minutes at room temperature. At this point, TMSOTf (28 mg, 0.12 mmol) was added, and the mixture was further stirred for 15 minutes, yielding a pale yellow solution. The solution was filtered through a syringe filter, and concentrated under vacuum. A 10 mL portion of Et_2O was then added to precipitate the product as a yellow powder. This precipitate was filtered and washed with hexanes (3 x 10 mL) to afford [**1b**][OTf] (70 mg, 74% yield). Orange-yellow needle shaped single crystals were obtained by vapor diffusion of Et_2O into a CH_3CN solution of [**1b**][OTf]. ^{1}H NMR (500 MHz, $CDCl_3$) δ 8.64 (d, *J* = 9.3 Hz, 2H), 8.44 – 8.36 (m, 2H), 8.07 (t, *J* = 8.2 Hz, 1H), 7.95 (m, 2H), 7.88 – 7.82 (m, 2H), 7.78 (d, *J* = 8.6 Hz, 2H), 7.53 (dd, *J* = 8.11, 4.55 Hz, 1H), 4.95 (s, 3H), 2.68 – 2.54 (m, 2H), 1.01 (m, 12 H) **^{13}C{^{1}H} NMR** (126 MHz, $CDCl_3$) δ 160.6,142.2, 140.1 (d, $^1J_{C\text{-}P}$ = 11.6 Hz), 139.5, 134.8, 134.4, 132.7, 132.3, 131.5, 130.6, 128.6, 128.0, 127.4, 121.7, 119.5, 40.0, 27.9 (d, $^1J_{C\text{-}P}$ = 35.1 Hz), 20.6, 19.7. **^{31}P{^{1}H} NMR** (162 MHz, $CDCl_3$) δ 48.4 **Elemental Analysis** calc'd for $C_{27}H_{29}AuBClF_3NO_3PS$: C: 42.23; H: 3.81. found: C: 41.87; H: 3.86.

Synthesis of [**2b**][OTf]

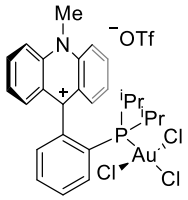

[**2b**][OTf] (50 mg, 0.06 mmol) was dissolved in acetonitrile (2 mL) in a 20 mL scintillation vial wrapped in aluminum foil, under nitrogen atmosphere. $PhICl_2$ (45 mg, 0.161 mmol) was added and the solution was stirred for 30 minutes in the dark. A 10 mL portion of Et_2O was then added to precipitate a pale-yellow powder. This precipitate was isolated by filtration and washed with hexanes (3 x 5 mL) and Et_2O (3 x 5 mL) to afford 43.0 mg of [**2b**][OTf] (yield: 75%). Yellow needle shaped single crystals were obtained by layering Et_2O on a CH_3CN solution of [**3**][OTf]. **^{1}H NMR** (500 MHz, CD_3CN): δ 8.63 (d, *J* = 9.3 Hz, 2H), 8.42 (m, 2H), 8.22 (m, 1H), 8.13 – 8.00 (m, 2H), 7.87 (dd, *J* = 8.8, 6.8 Hz, 2H), 7.82 – 7.72 (m, 3H), 4.89 (s, 3H), 2.85 (m, 2H), 1.53 – 1.30 (m, 12H).**^{13}C{^{1}H} NMR** (126 MHz, CD_3CN) δ 157.3, 142.7, 140.2, 138.0, 137.5, 135.1, 134.3, 133.83, 130.4, 129.5, 127.6, 125.9 (d, $^1J_{C\text{-}P}$ = 52.7 Hz), 119.60, 40.15, 30 (d, $^1J_{C\text{-}P}$ = 26.9 Hz), 20.6. **^{31}P{^{1}H} NMR** (162 MHz, CD_3CN) δ: 63.0 **Elemental Analysis** calc'd for $C_{27}H_{29}AuBCl_3F_3NO_3PS$: C: 38.66; H: 3.48. found: C: 38.44; H: 3.61.

2 NMR spectra

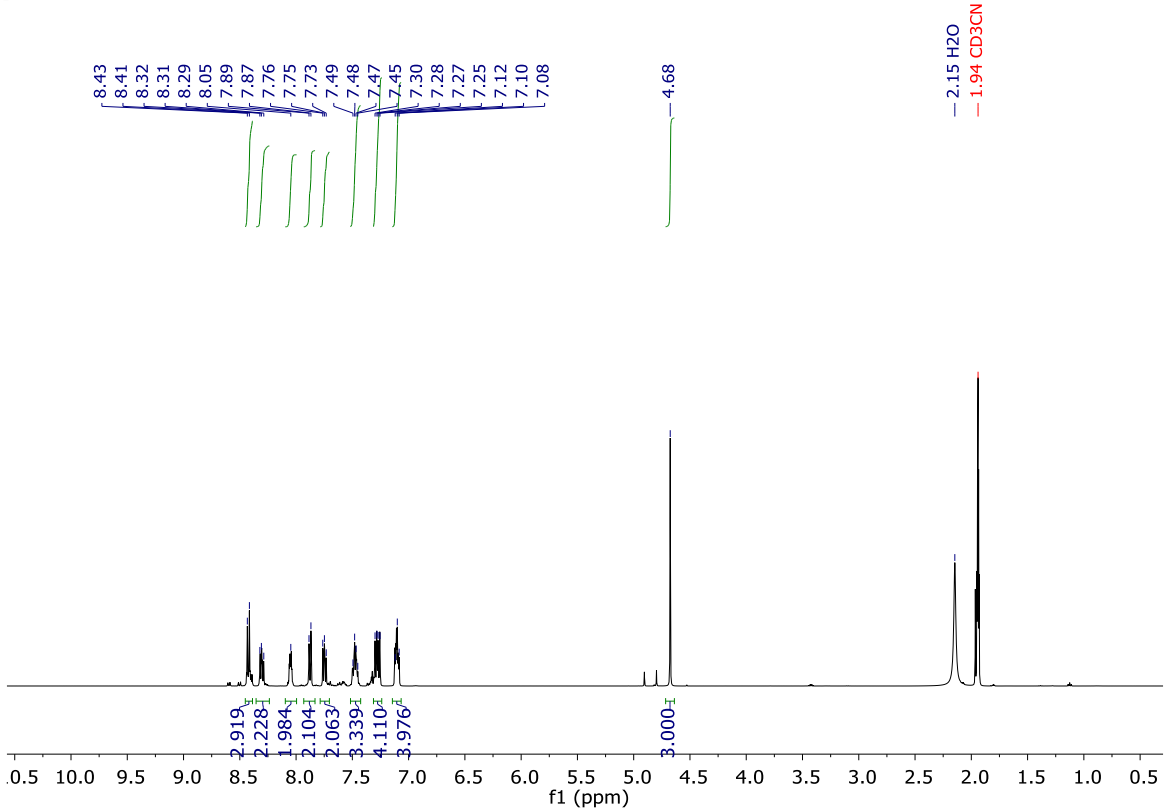

Figure S1. ^{1}H NMR spectrum of [**2a**][BF_4] in CD_3CN

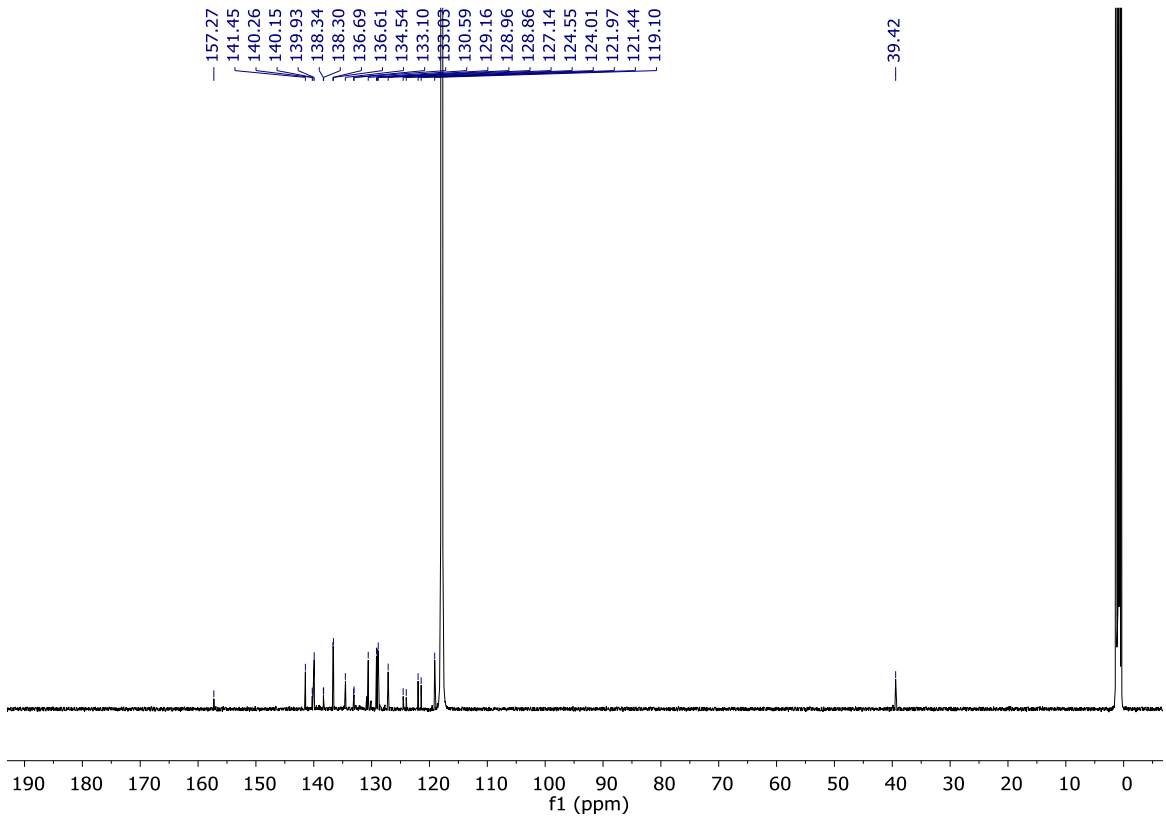

Figure S2. $^{13}C\{^{1}H\}$ NMR spectrum of [**2a**][BF_4] in CD_3CN. The solvent peak is truncated.

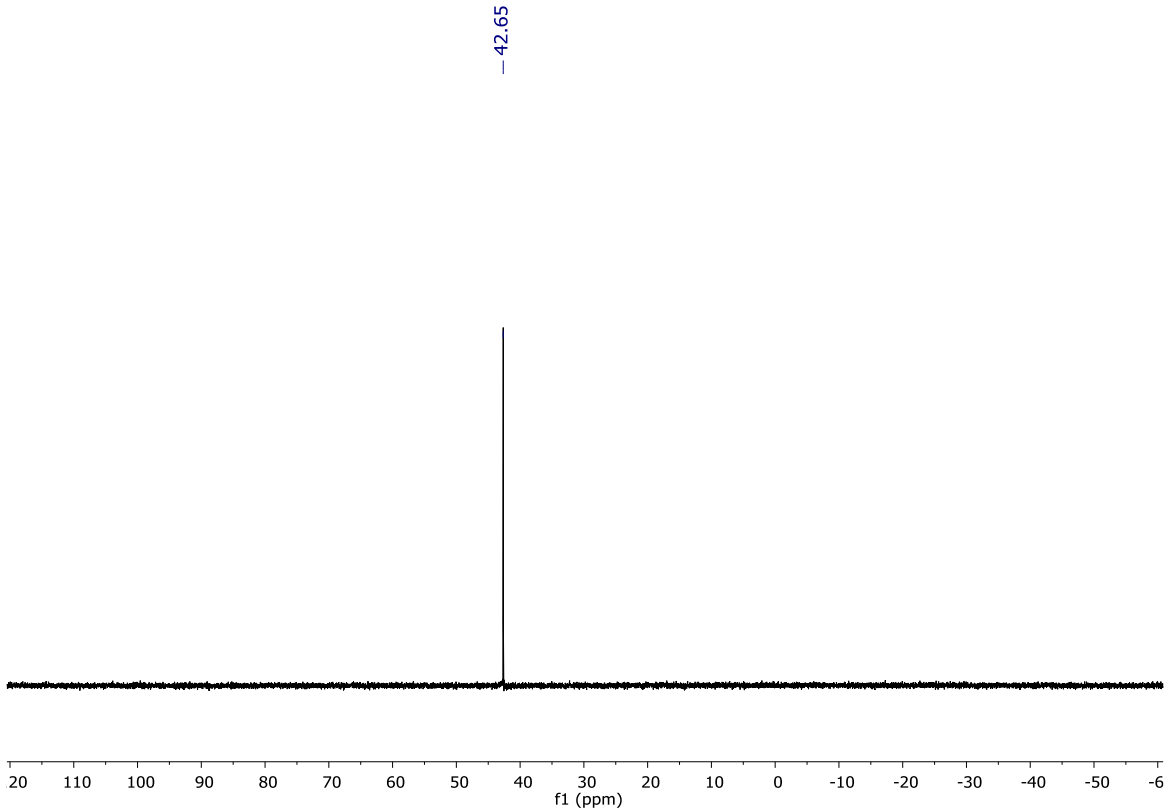

Figure S3. $^{31}P\{^{1}H\}$ NMR spectrum of [**2a**][BF_4] in CD_3CN

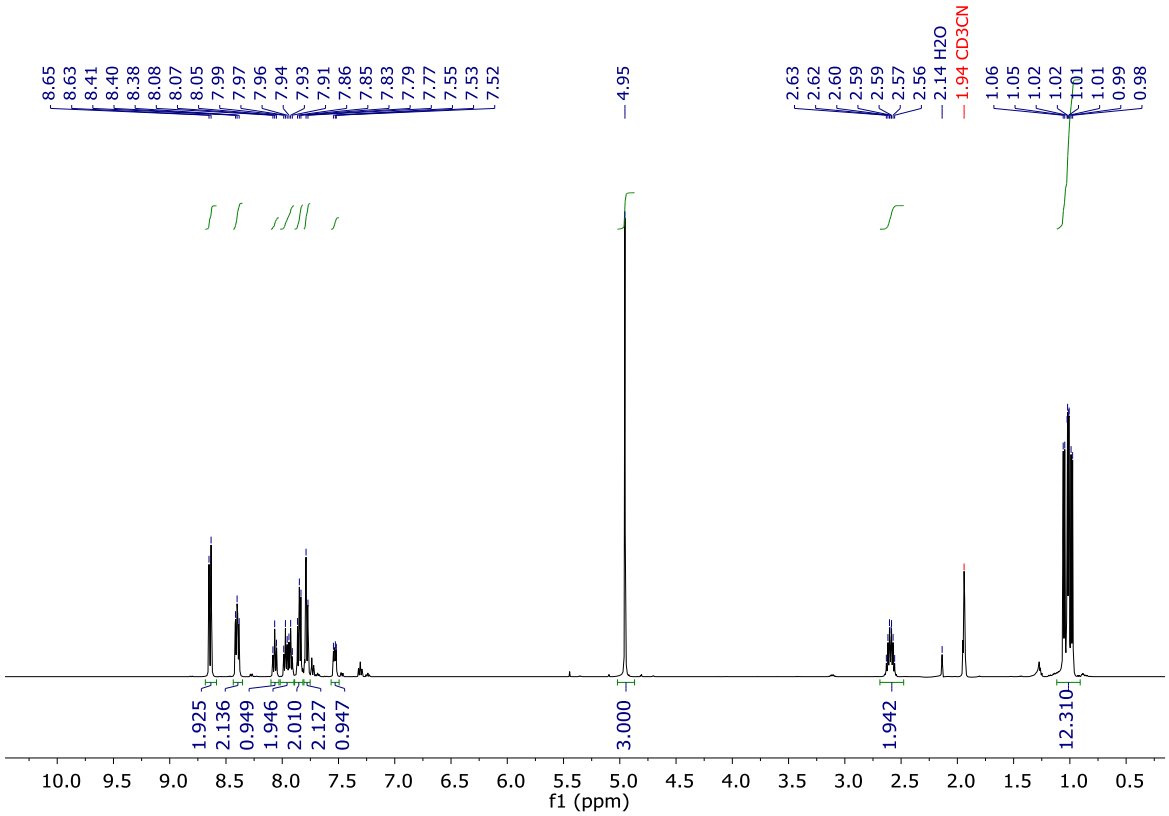

Figure S4. ^{1}H NMR spectrum of [**1b**][OTf] in CD_3CN

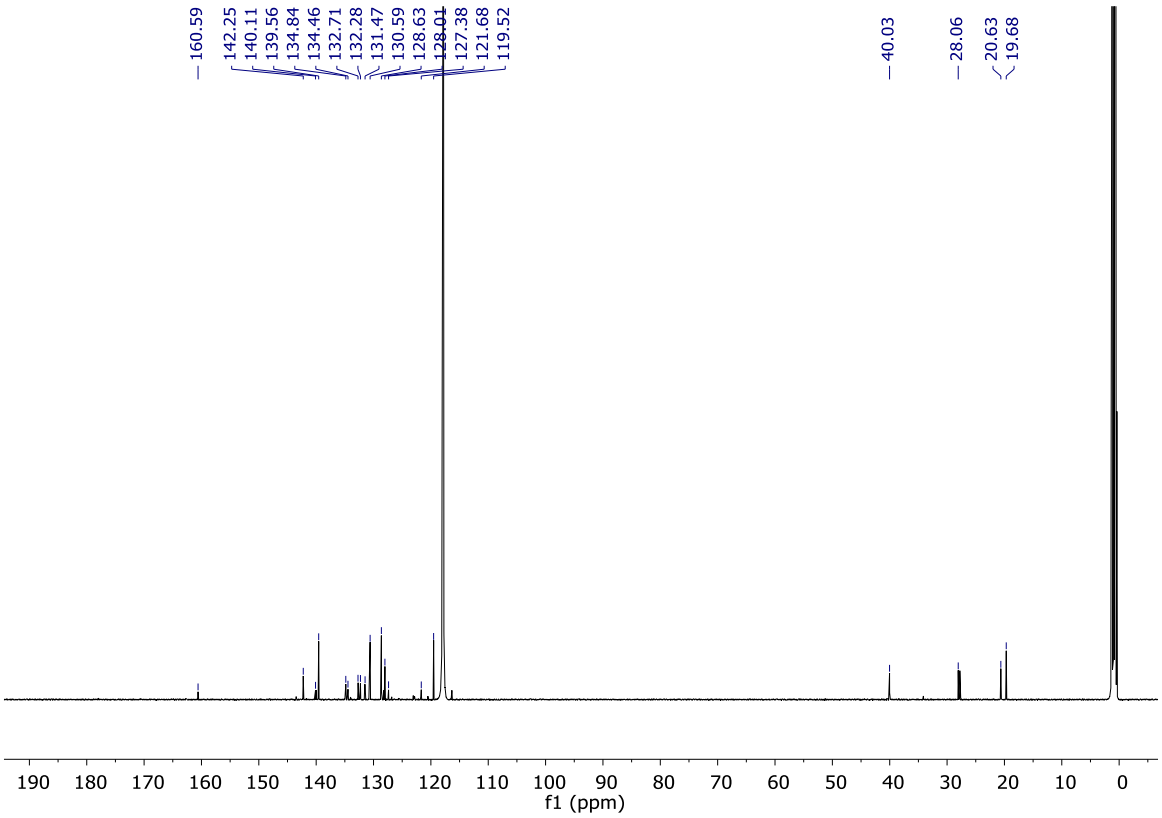

Figure S5. $^{13}C\{^{1}H\}$ NMR spectrum of [**1b**][OTf] in CD_3CN. The solvent peak is truncated.

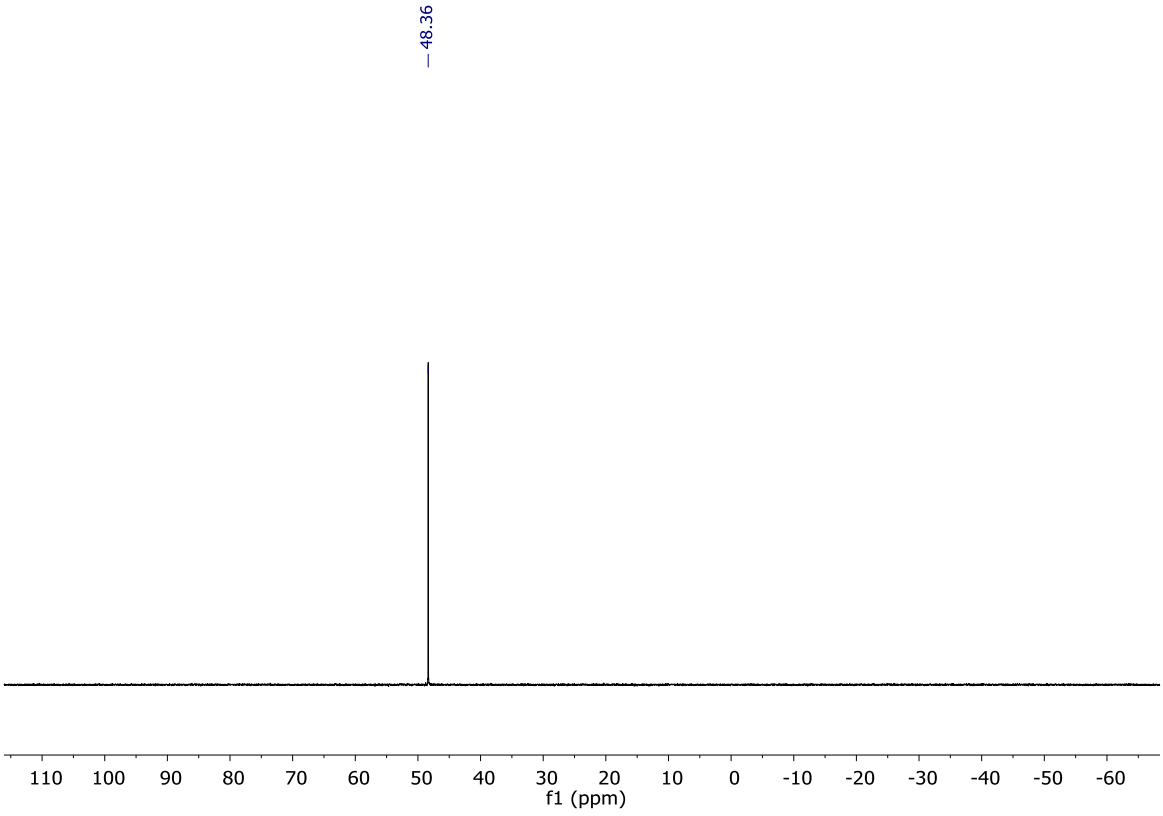

Figure S6. $^{31}P\{^{1}H\}$ NMR spectrum of [**1b**][OTf] in CD_3CN

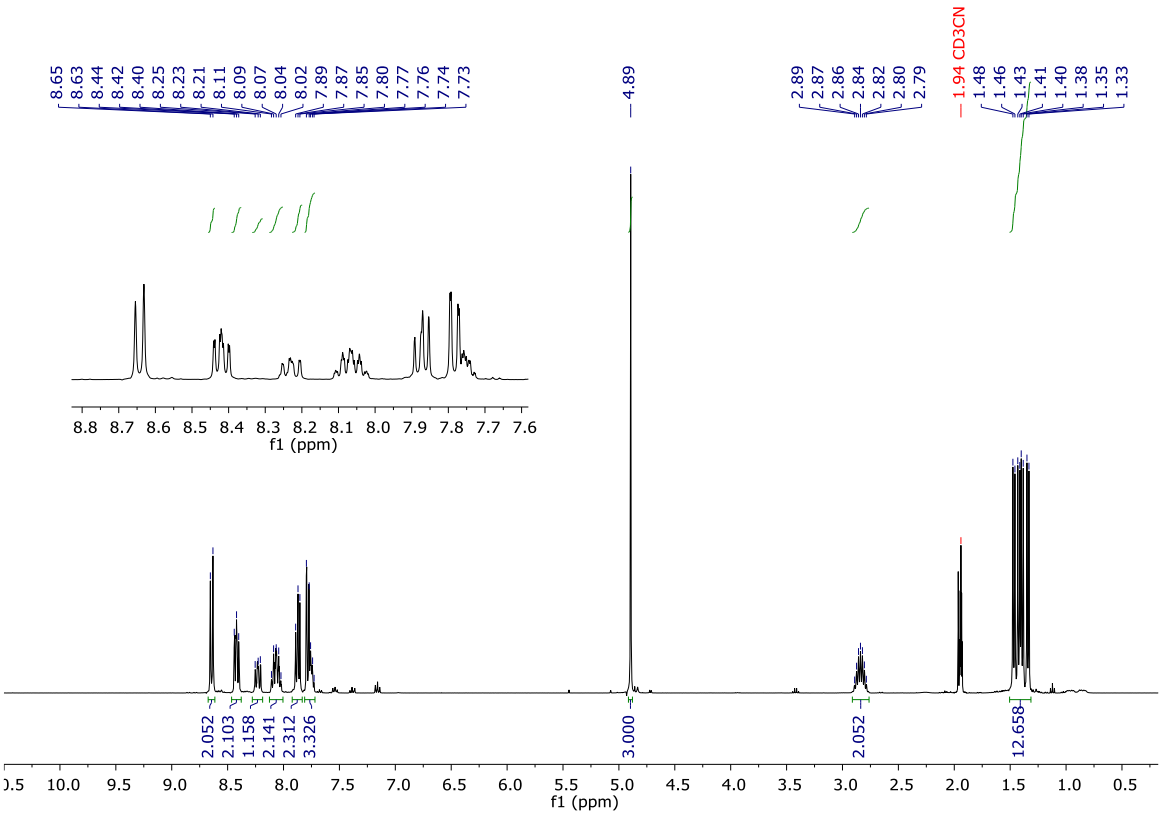

Figure S7. ^{1}H NMR spectrum of [**2b**][OTf] in CD_3CN

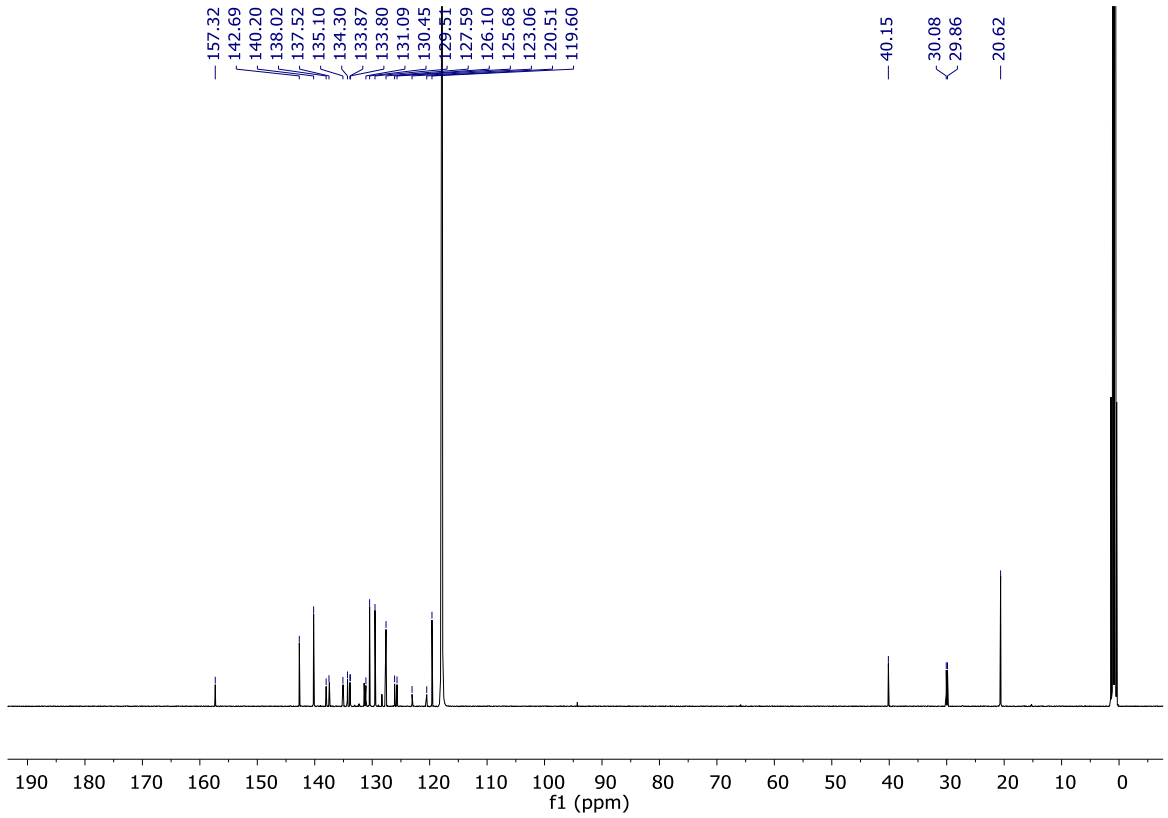

Figure S8. $^{13}C\{^{1}H\}$ NMR spectrum of [**2b**][OTf] in CD_3CN. The solvent peak is truncated.

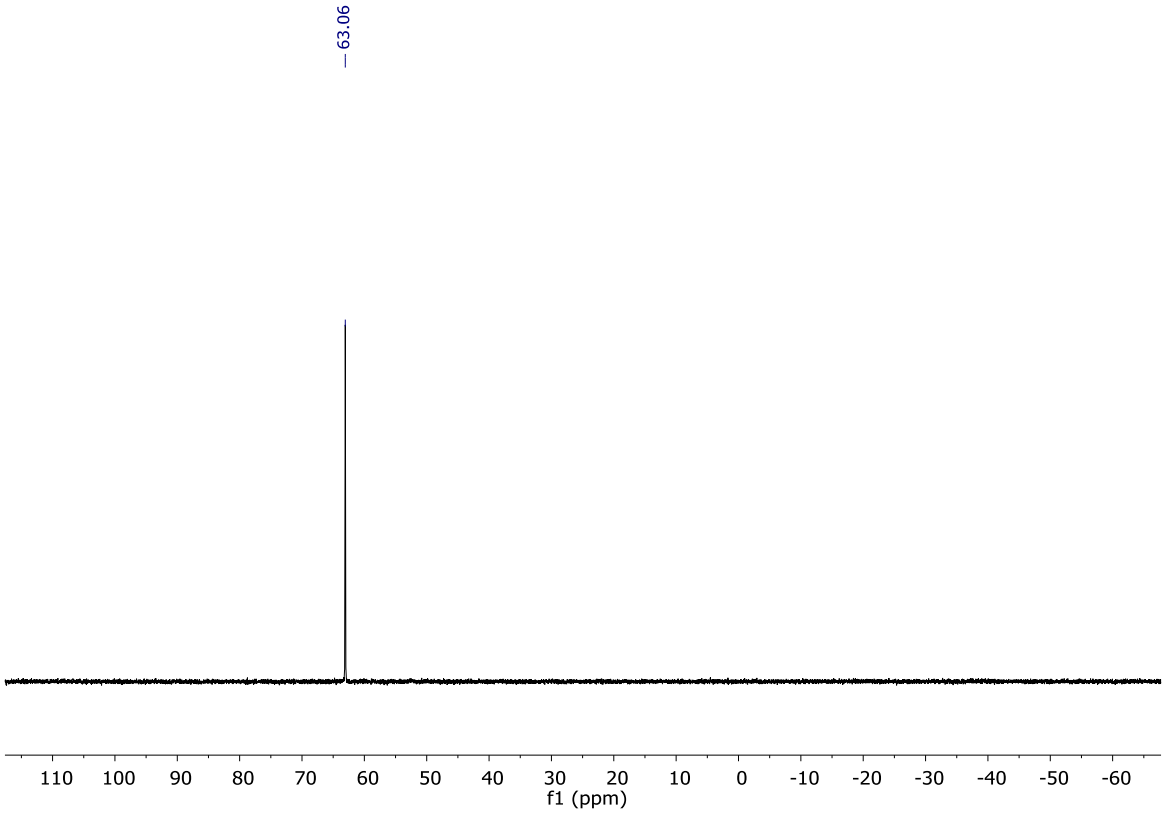

Figure S9. $^{31}P\{^{1}H\}$ NMR spectrum of [**2b**][OTf] in CD_3CN

3 UV-vis spectroscopy

UV-Vis absorbance measurements were performed on a Shimadzu UV-2502PC UV-Vis spectrophotometer. Spectra were collected at a concentration of 5 x 10^{-4} M in acetonitrile using a 1mm quartz cuvette. The emission profile of the green LEDs implemented in this study was obtained using a PTI QuantaMaster 40 fluorescence spectrophotometer (Figure S13).

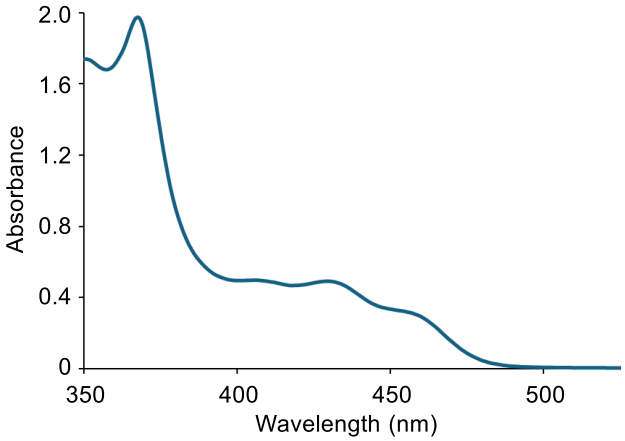

Figure S10. UV-vis spectrum of [**2a**][BF_4] in MeCN.

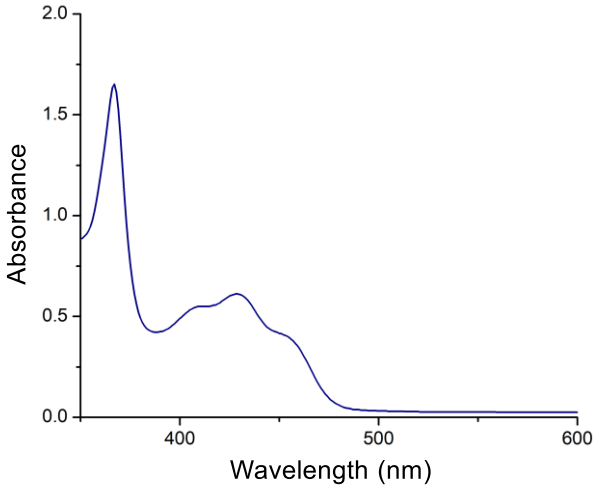

Figure S11. UV-vis spectrum of [**1b**][OTf] in MeCN

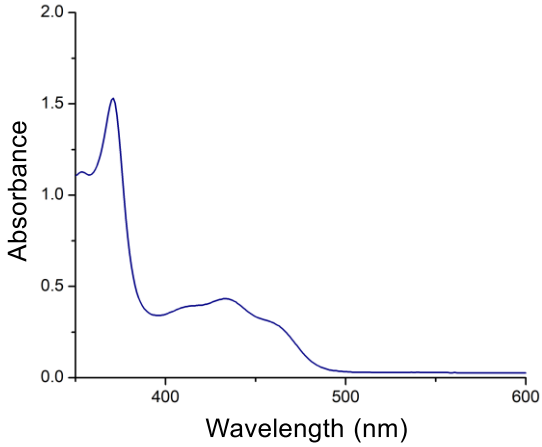

Figure S12. UV-vis spectrum of [**2b**][OTf] in MeCN

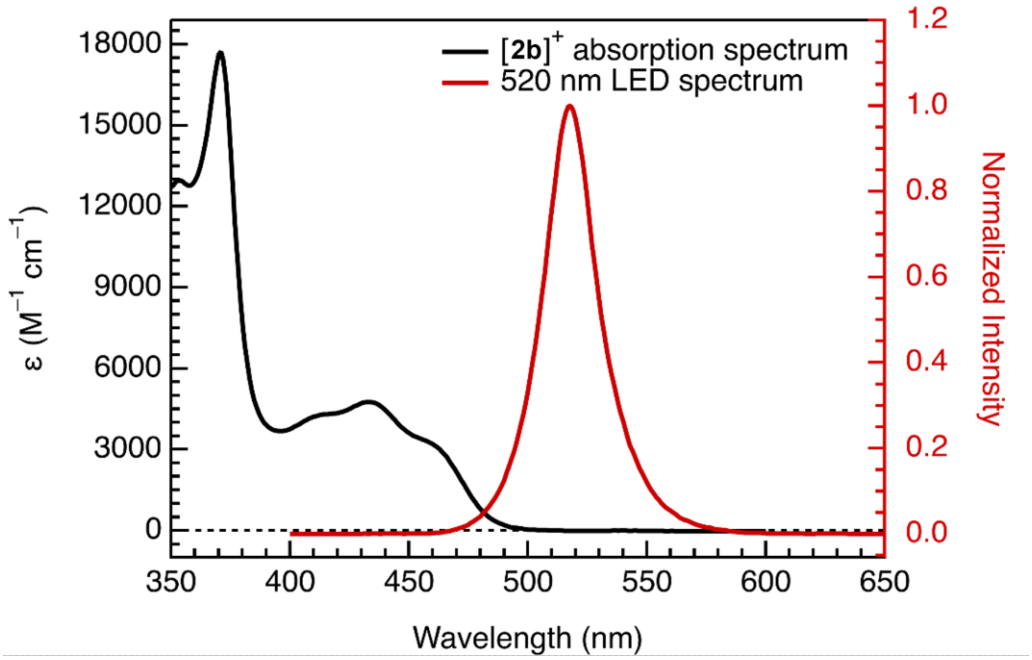

Figure S13. Emission profile of the 520 nm green LEDs used in this work, coplotted with the absorption spectrum of [**2b**]$^{+}$.

4 Photolysis studies

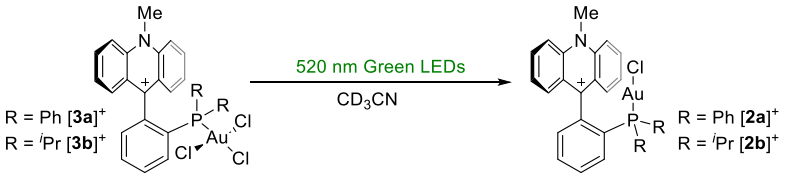

Solution state photolysis

In a typical experiment, an NMR tube was charged with [**2a**][BF_4] or [**2b**][OTf] (10 mg, 0.012 mmol) in a glove box. Dry CD_3CN (0.6 mL) was then added along with a capillary containing H_3PO_4. For trap-free photolysis reactions, cyclohexene (3 µL, 0.03 mmol) was also added. The tube was sealed and the solution was irradiated using green LEDs. $^{31}P\{^1H\}$ spectra were recorded periodically (Figure S14-S17). The final solution was subjected to GC-MS analysis (Figure S18-S19).

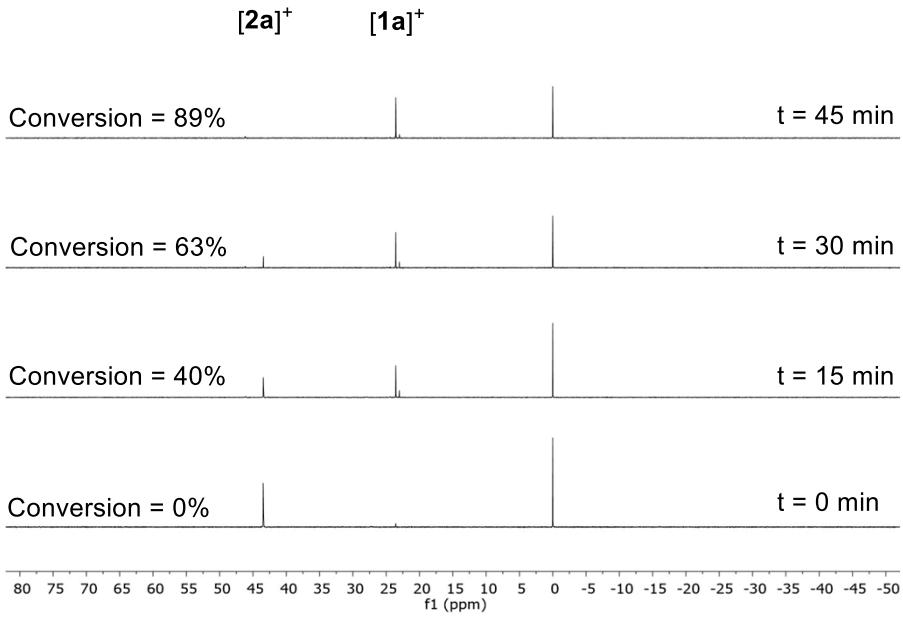

Figure S14. $^{31}P\{^1H\}$ NMR spectral changes during the photolysis of [**2a**][BF_4] in CD_3CN (light source: 520 nm green LEDs).

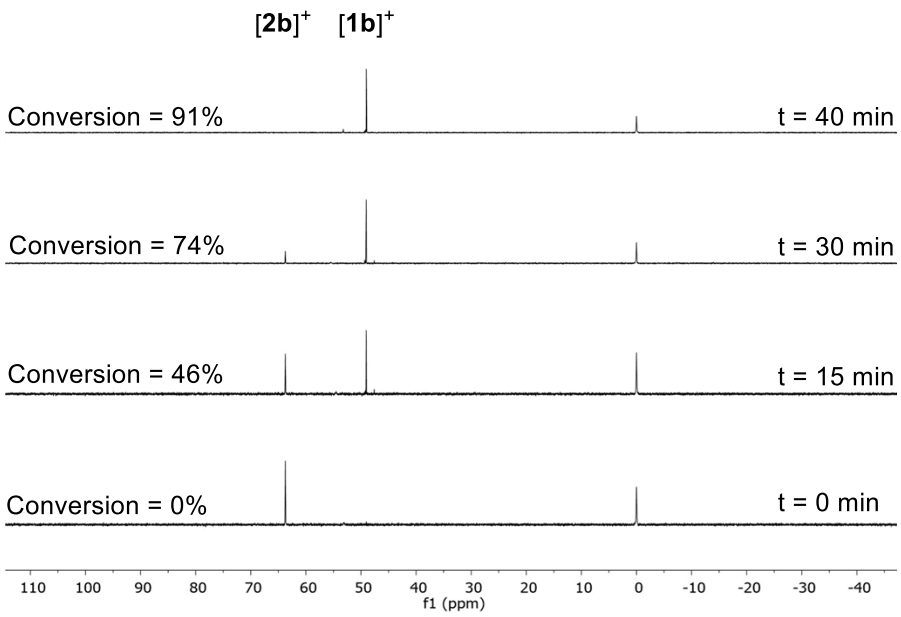

Figure S15. $^{31}P\{^{1}H\}$ NMR spectral changes during the photolysis of [**2b**][OTf] in CD_3CN (light source: 520 nm green LEDs).

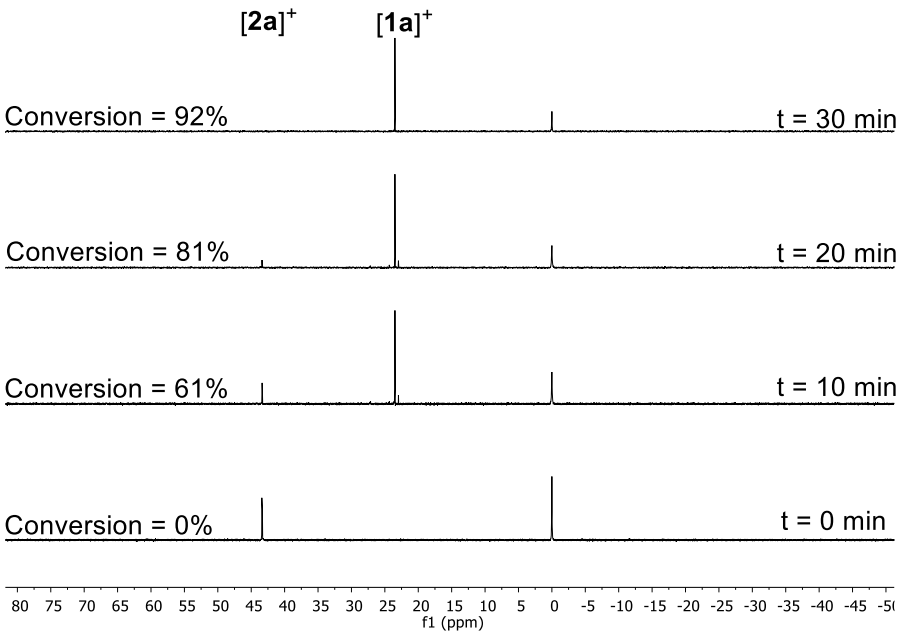

Figure S16. $^{31}P\{^{1}H\}$ NMR spectral changes during the photolysis of [**2a**][BF_4] in CD_3CN using 2.5 equiv of cyclohexene (light source: 520 nm green LEDs).

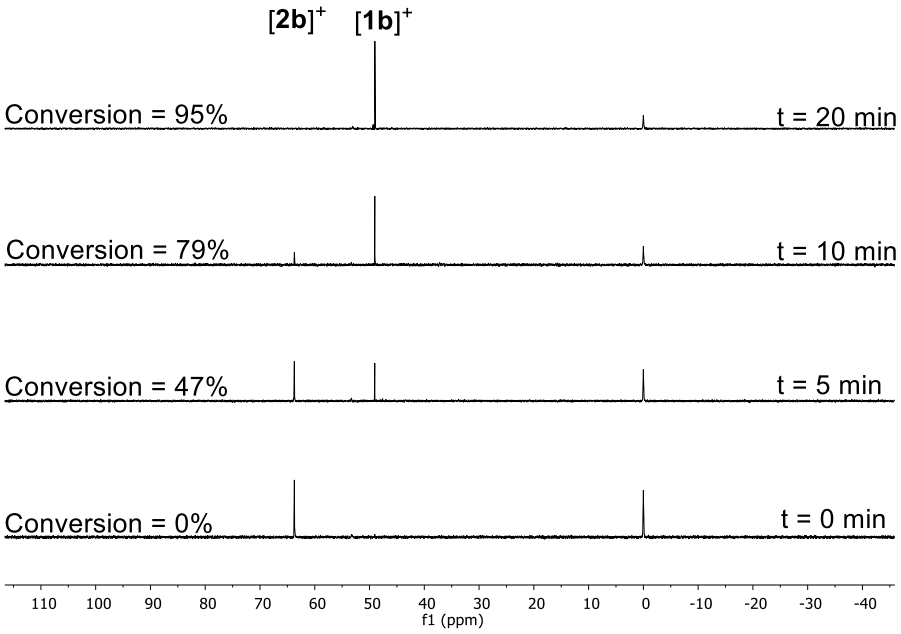

Figure S17. $^{31}P\{^{1}H\}$ NMR spectral changes during the photolysis of [**2b**][OTf] in CD_3CN using 2.5 equiv of cyclohexene (light source: 520 nm green LEDs).

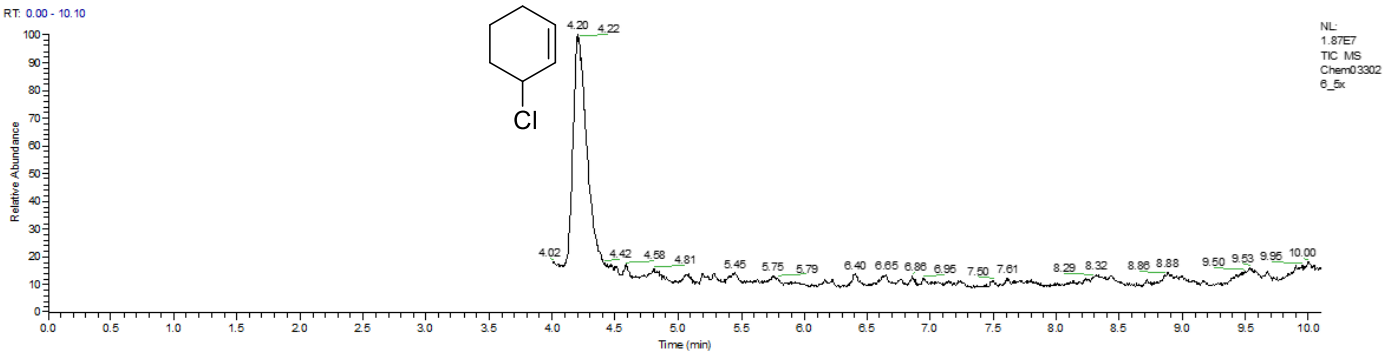

Figure S18. Gas chromatogram of a solution of [**2a**][BF_4] photolyzed in the presence of 10 equiv cyclohexene.

Solid state photolysis

In a typical experiment, a solution of [**2b**][OTf] (5 mg, 0.006 mmol) was drop-casted onto a glass slide and dried under a stream of nitrogen. The solid film was irradiated with green LEDs for 5 hours and $^{31}P\{^{1}H\}$ spectra were recorded periodically (Figure S15) by redissolving the compound back in CD_2Cl_2.

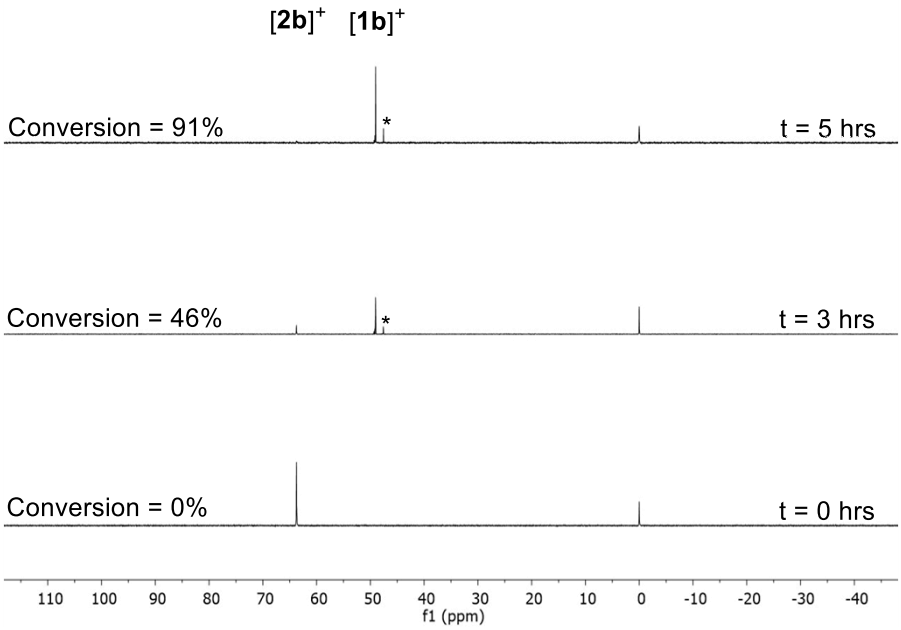

Figure S19. $^{31}P\{^{1}H\}$ NMR spectral changes during the solid state photolysis of [**2b**][OTf] in CD_2Cl_2 (light source: 520 nm green LEDs). The side product marked by a star is tentatively assigned to the phosphine oxide.

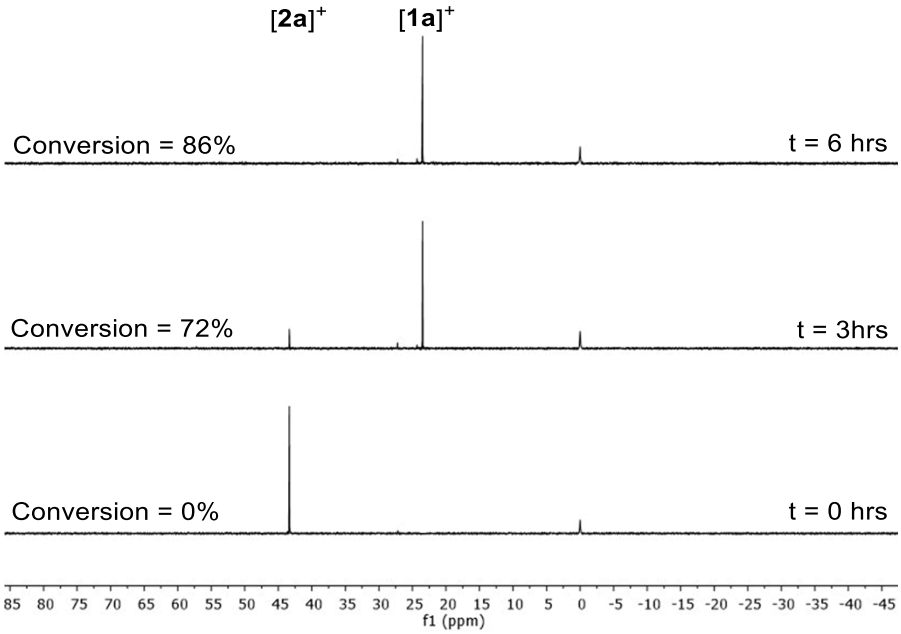

Figure S20. $^{31}P\{^{1}H\}$ NMR spectral changes during the solid state photolysis of [**2a**][BF_4] in CD_2Cl_2 (light source: 520 nm green LEDs).

5 Quantum yield measurements

Photochemical quantum yield measurements were carried out following a previously published procedure using azobenzene as the chemical actinometer.[2] In this method, the photoisomerization of *trans*-azobenzene to *cis*-azobenzene is used to determine the photon flux crossing the reaction medium, and conversion of the analyte is monitored under conditions identical to the actinometer.

Photoisomerization of *trans*-azobenzene: A semi-micro quartz cell (with a 1 cm path length and 2 mm internal width) was loaded with *trans*-azobenzene (0.07 M) in CD_3CN (0.6 mL) and irradiated using green LEDs (λ_{max} = 520 nm) from LemonBest with an electrical power of 5W. The isomerization of *trans*-azobenzene to *cis*-azobenzene was monitored by periodically recording ^1H NMR spectra. The rate of the reaction follows the equation:

$$dC_{cis}/dt = -dC_{trans}/dt = \Phi.L_{abs} \quad (1)$$

$$dC_{cis}/dt = -dC_{trans}/dt = I_0 \times \Phi_{t\to c} \times (1\text{-}10^{-\epsilon t \cdot b \cdot Ctrans}) - I_0 \times \Phi_{c\to t} \times (1\text{-}10^{-\epsilon c \cdot b \cdot Ccis}) - k \times c_{cis} \quad (2)$$

In this equation, I_0 is the light intensity, C_{trans} and C_{cis} are the concentrations of *trans*-azobenzene or *cis*-azobenzene respectively, $\Phi_{t\to c}$ and $\Phi_{c\to t}$ are the photochemical quantum yields of the photoisomerization from the trans to the cis isomer, and from the cis to the trans isomer respectively, ϵt and ϵc are the molecular absorption coefficients of the trans and the cis forms respectively, and *b* is the length of the light path.

At t = 0, C_{cis} = 0 and the term (1 - $10^{-\epsilon c \cdot b \cdot Ccis}$) becomes negligible. Also, C_{trans} is chosen to be high enough to ensure total absorption of incident photons, rendering the term $10^{-\epsilon t \cdot b \cdot Ctrans}$ negligible. Therefore, equation *(2)* may be simplified to:

$$dC_{cis}/dt = -dC_{trans}/dt = I_0 \times \Phi_{t\to c} \quad (3)$$

Now equation *(3)* can be regarded as a 1st order rate law, where at t = 0, the initial slope of the concentration of *cis*-azobenzene versus time (Figure S16) is equal to $I_0 \times \Phi_{t\to c}$. Nonlinear fitting analysis of the C_{cis} versus t graph at t = 0 then gives the desired photon flux I_0.

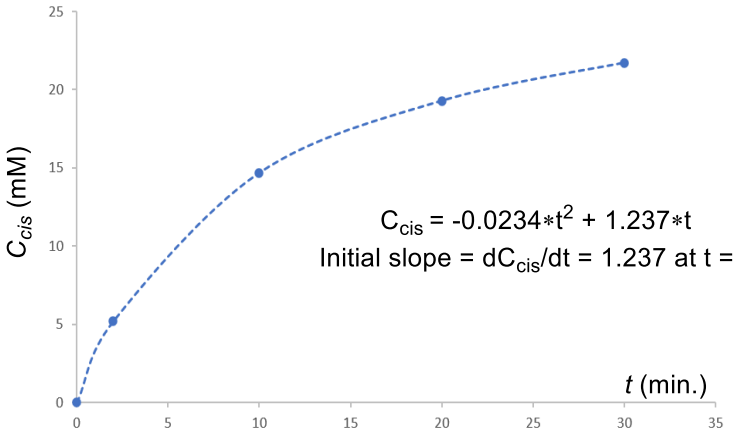

Figure S21. Non-linear fit of the concentration of *cis*-azobenzene versus time. The initial slope is 1.237 at t = 0.

Photoreduction of [**2b**][OTf] and [**2a**][BF_4]:
The same semi-micro quartz cell mentioned earlier was loaded with a solution of the Au(III) complex (13.8 mM) and different equivalents of cyclohexene in CD_3CN (0.6 mL). The trap concentration was varied from 2.5 eq to 25 eq. The resulting solution was irradiated using the same light source and with the sample positioned exactly the same way as the actinometer relative to the light source. The photolysis was monitored by periodic recording of $^{31}P\{^1H\}$ and ^1H NMR spectra, and the integration of the peaks in these spectra was used to determine the change in concentration (ΔCu). The photochemical quantum yields were calculated according to equation *(4)*:

$$\Phi_u = \Phi_{t\to c} \times (\Delta C_u/\Delta t_u) \times (dt/dC_{cis}) \quad (4)$$

where Φ_u is the quantum yield of the photolysis of [**2b**][OTf] or [**2a**][BF_4], ΔC_u is the change in concentration of the irradiated solution, and Δt_u is the irradiation time. dC_{cis}/dt is the slope at t = 0 obtained through the

nonlinear fitting analysis of the actinometer as explained above. In acetonitrile, $\Phi_{t\rightarrow c}$ is 0.28 at 524 nm.[3] The irradiation time Δt_u was set to 3 min.

Table S1. Quantum yield of photolysis of [**2a**][BF_4] in the presence of various concentrations of cyclohexene

Eq. of trap	ΔC(Change in conc.)	Δt	Φ_u(%)
0	0.69 mM	3min	5.2%
2.5	0.81 mM	3min	6.1%
4	1.10 mM	3min	8.3%
9	1.37 mM	3min	10.4%
19	2.17 mM	3min	16.7%
25	2.51 mM	3 min	18.9%

Table S2. Quantum yield of photolysis of [**2b**][OTf] in the presence of various concentrations of cyclohexene

Eq. of trap	ΔC(Change in conc.)	Δt	Φ_u(%)
0	0.79 mM	3min	5.8%
2.5	1.05 mM	3min	7.9%
4	1.21 mM	3min	9.1%
9	1.68 mM	3min	12.7%
19	2.45 mM	3min	18.6%
25	2.72 mM	3min	20.5%

6 Transient Spectroscopy

6.1. General considerations for Nanosecond TA Spectroscopy (nsTA)

Broadband nanosecond TA spectroscopy (nsTA) was performed using an EOS TA spectrometer (Ultrafast Systems). The EOS is a probe-referenced TA spectrometer that produces 100 ps broadband probe pulses in the range of 350–900 nm, generated by a laser pumped photonic crystal fiber internal to the instrument. Excitation pulses were furnished by a 50 Hz, diode-pumped, pulse Nd:YAG laser system with an integrated optical parametric oscillator (NT230-50, Ekspla) with an average pulse width of ~4 ns and focused into the sample, achieving a spot size of ~1 mm at the sample position. Pump and probe pulses were overlapped at the sample position in a typical narrow angle geometry. The time delay between the pump and probe pulses is electronically controlled with the spectrometer receiving electronic trigger signals from the laser. Samples were prepared in a nitrogen-filled glovebox and sealed in 2 mm path length cuvettes.

6.2. General considerations for Femtosecond TA Spectroscopy (fsTA)

Femtosecond TA spectroscopy (fsTA) was carried out using a HARPIA (Light Conversion) TA system coupled to a Yb:KGW laser (Pharos, Light Conversion) with a 1030 nm fundamental which furnishes <100 fs pulses at a repetition rate of 50 kHz and a per pulse energy of 400 µJ. Pump pulses were generated by pumping an Orpheus Neo OPA (Light Conversion), with 340 µJ of the 1030 fundamental. Femtosecond probe pulses were generated

by pumping either Sapphire (5 mm) or YAG (10 mm) crystals with 24 μJ of the 1030 nm fundamental. Continuum generation from sapphire furnished probe pulses in the region from 450-850 nm. UV-visible probe pulses between 350-550 nm were obtained by pumping sapphire with the second harmonic (SH) of the fundamental (515 nm) generated via a type I β-barium borate (BBO) crystal. Pump pulses were polarized using a Berek's compensator to achieve a polarization of 54.7˚ relative to the probe pulse. Both pump and probe pulses were subsequently focused onto the sample to achieve spot sizes of ~100 μm, with the pump slightly larger than the probe. Time delays were achieved by delaying the probe pulse with respect to the pump on a quadruple pass delay line with a maximum time delay of 6 ns. TA spectra were obtained by averaging 1000 spectra at each time delay. Data was chirp-corrected and processed using the CarpetView software (Light Conversion), which was also used for global analysis to obtain EAS and their time evolution. In addition, TA spectra in UV and visible probe regions were collected on the same, and under the same conditions and were merged at 500 nm post processing using CarpetView. Time constants for single wavelength kinetics were obtained by least-squares fitting to the convolution of an Instrument Response Function (IRF) and a sum of exponentials according to:

$$f(t) = IRF * \sum_{i=1}^{n} A_i \times exp[-\frac{t - t_0}{\tau_0(i)}] + y_0$$

UV-vis spectra were taken for all species subjected to fsTA excitation before and after excitation.

6.3. Transient Spectroscopy Data

6.3.2. TA on [1a][BF_4]

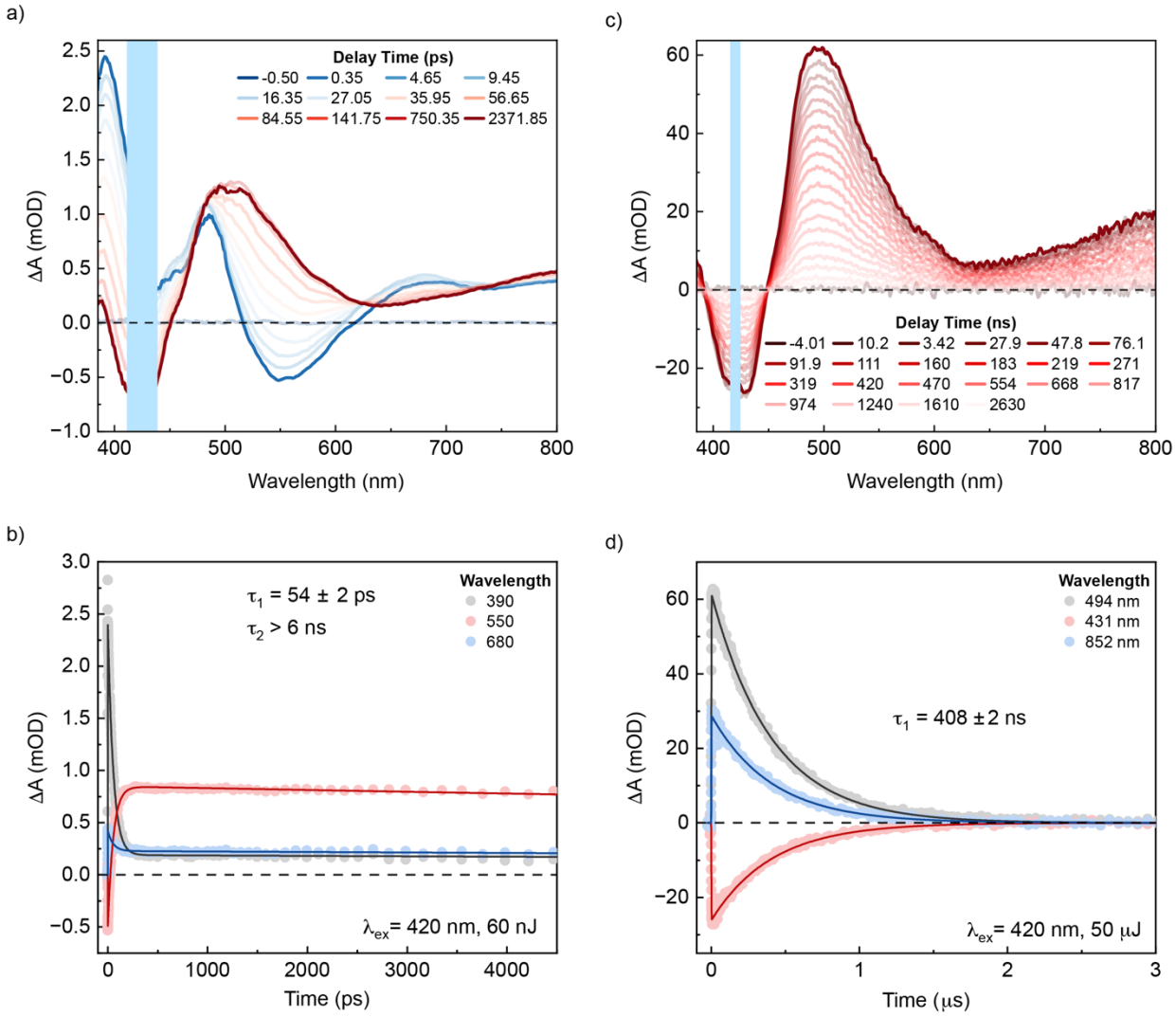

Figure S22. a) Femtosecond TA data of 173 μM [**1a**][BF_4] in MeCN circularly flowed at 2 mL/min. b) Representative kinetic traces and global fits of data shown in a. c) Nanosecond TA data of 173 μM [**1a**][BF_4] in MeCN circularly flowed at 2 mL/min. d) Representative kinetic traces and global fits of data shown in c.

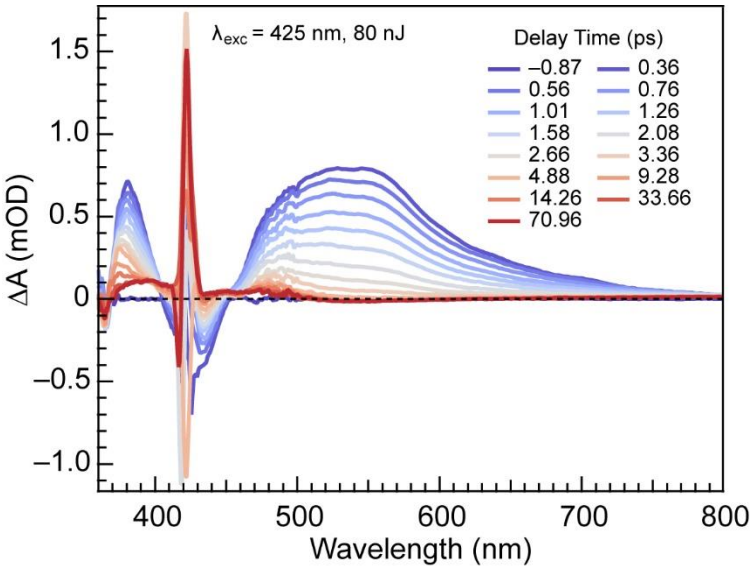

Figure S23. Femtosecond TA data of compound EliPhos in MeCN.

6.5. UV-visible absorption spectroscopy

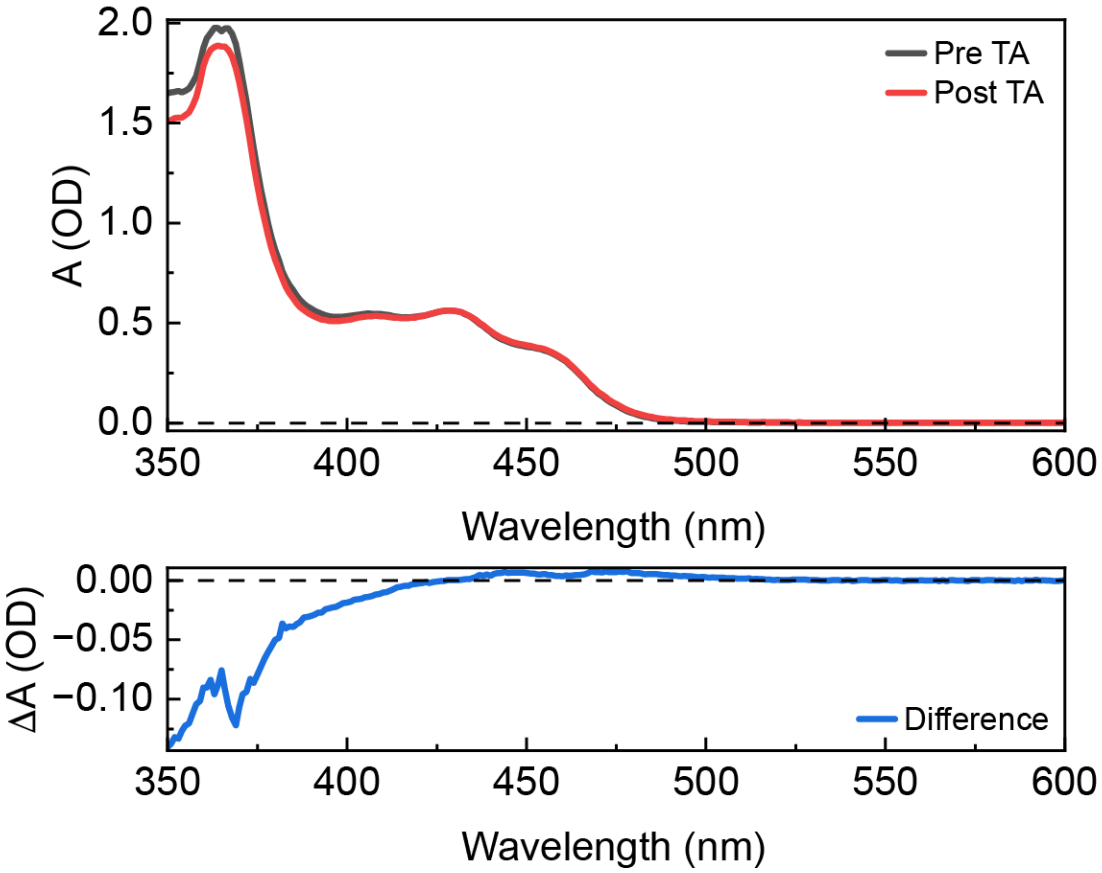

Figure S24. UV-visible absorption spectra of 114 µM [**2a**][BF_4] pre and post TA in MeCN and their difference spectra.

6.5. Stern-Volmer analysis of [2a][BF_4] in the presence of cyclohexene

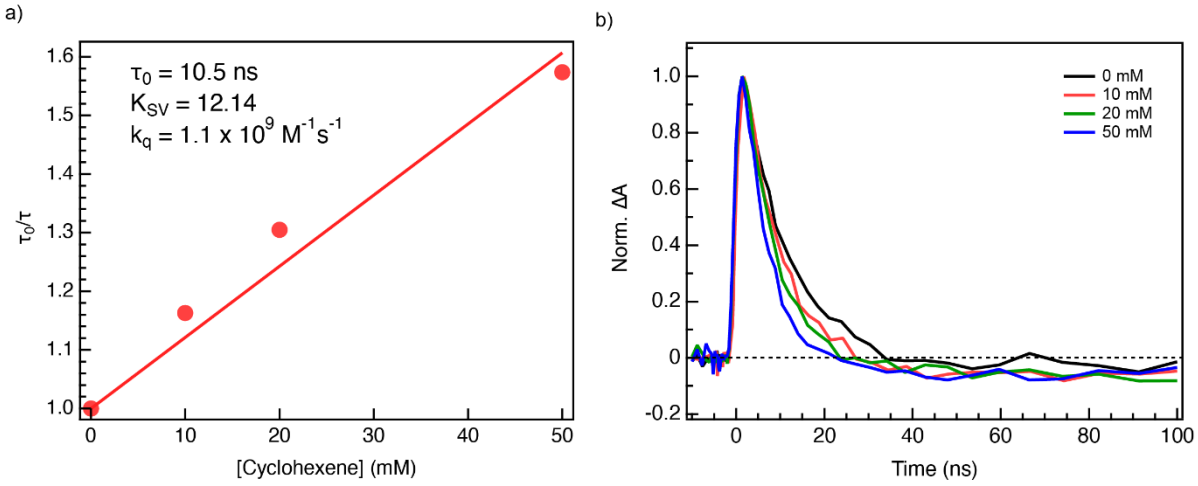

Figure S25. a) Stern-Volmer Analysis of [**2a**][BF_4] obtained from the fit of the kinetic traces in b. b) Nanosecond TA kineticat 390 nm of [**2a**][BF_4] in the presence of varying amounts of cyclohexene circularly flowed at 2 mL/min.

7 Catalysis Study

Hydroarylation of **3**:

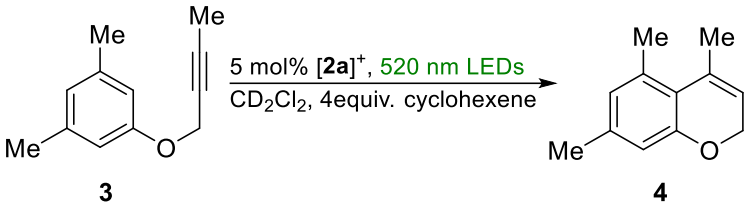

3 **4**

Reaction with Cat. [**2a**][BF_4]: An NMR tube was loaded with **3** (40 mg, 0.230 mmol), [**2a**][BF_4] (9.7 mg, 0.012 mmol, 5 mol%), and cyclohexene (5 µL, 0.046 mmol, 20 mol%) in the dark under a nitrogen atmosphere. A ^{1}H NMR spectrum was recorded before irradiation, followed by green light irradiation for 30 minutes. The ^{1}H NMR spectrum confirms the formation of **4** with 47% conversion immediately after the end of irradiation. When the reaction was allowed to stand for another 60 minutes in the absence of light, conversion increased to 54%.

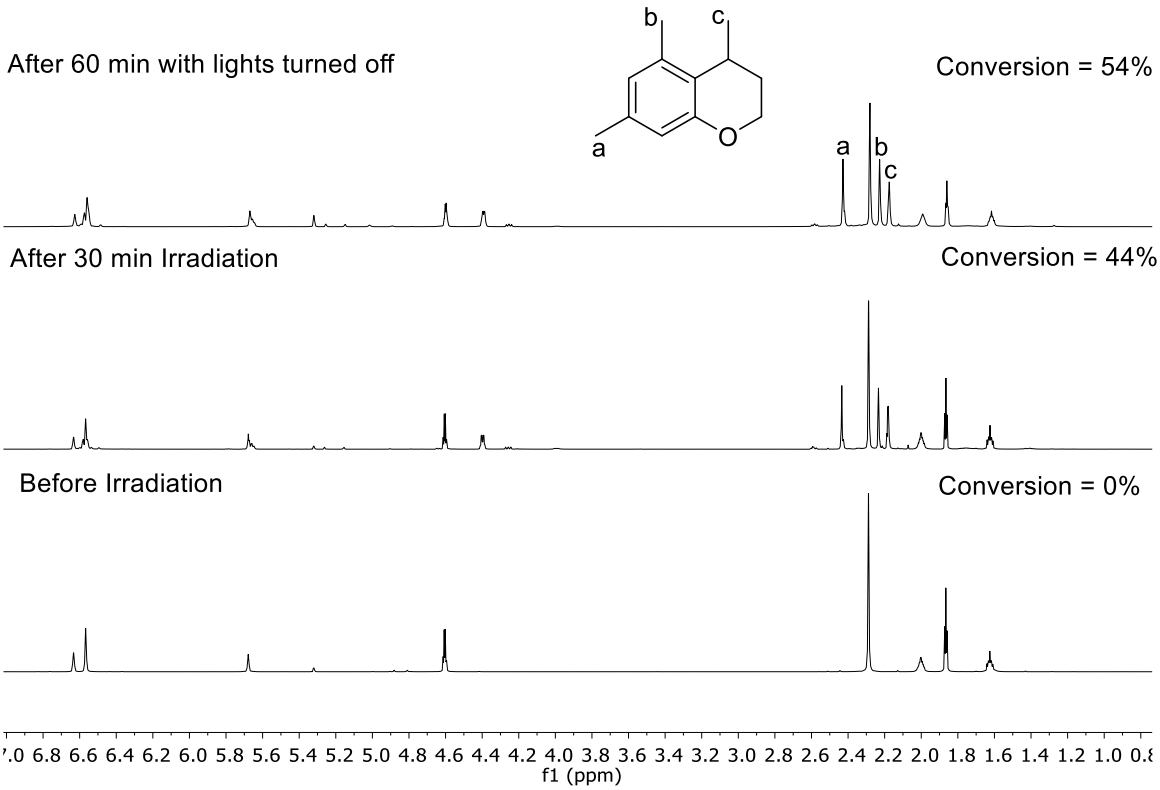

Figure S26. ^{1}H NMR spectra showing hydroarylation of **3** using [**2a**][BF_4] and cyclohexene as the precatalyst mixture.

8 Computational studies

8.1 General methods

The structures of [**2a**]$^{+}$, [**1b**]$^{+}$ and [**2b**]$^{+}$ were optimized by DFT methods as implemented in Gaussian 16 using the MPW1PW91 functional and a mixed basis set defined as follows: cc-pVTZ-PP for Au; 6-31G(d',p') for P/Cl; 6-31G(d') for C/N; 6-31G for H. Frequency calculations, performed using the same level of theory on the optimized geometries, resulted in no imaginary frequencies. Time-Dependent DFT (TD-DFT) calculations were conducted at the geometry optimized structures (using the same level of theory). Solvation was accounted for using a polarizable continuum model with acetonitrile as the solvent. The Kohn-Sham orbitals were visualized using the Avogadro program. NTO calculations were performed on the excited state using the same level of theory. UV-vis spectra were simulated by TD-DFT calculations and visualized using GaussSum 3.0.[4]

8.2 Simulated UV-vis spectra

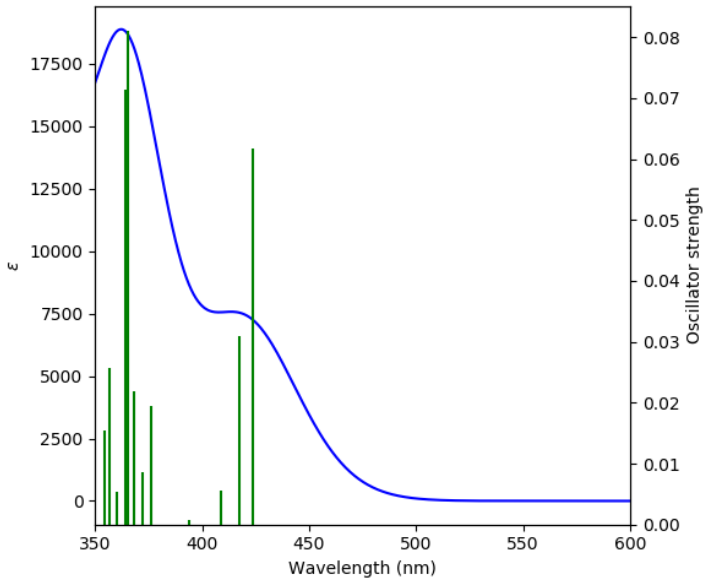

Figure S27. Simulated UV-vis spectrum of [**2a**]$^{+}$.

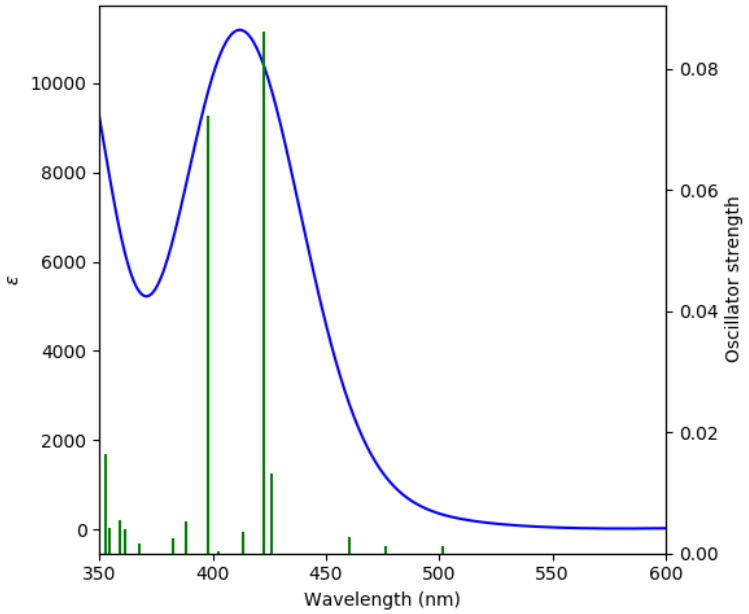

Figure S28. Simulated UV-vis spectrum of [**1b**]$^{+}$.

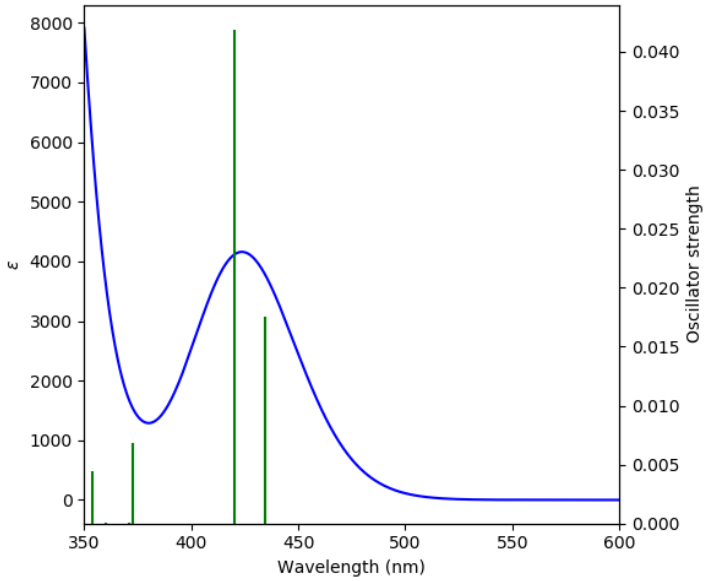

Figure S29. Simulated UV-vis spectrum of [**2b**]$^+$ in MeCN.

8.3 TD-DFT studies and relevant Kohn-Sham orbitals

Relevant vertical excitations obtained from the TD-DFT calculations on the optimized structures of [**1b**]$^+$, [**2a**]$^+$, and [**2b**]$^+$ along with the corresponding plots of the Kohn-Sham orbitals are provided below.

Table S3. Relevant vertical excitations for [**1b**]$^+$ calculated by TD-DFT

Excited State	Wavelength(nm)	Osc. Strength, f	Major and minor contributions
1	426.6	0.092	HOMO⟶LUMO (98%)
2	388.3	0.0068	HOMO-1⟶LUMO (99%)

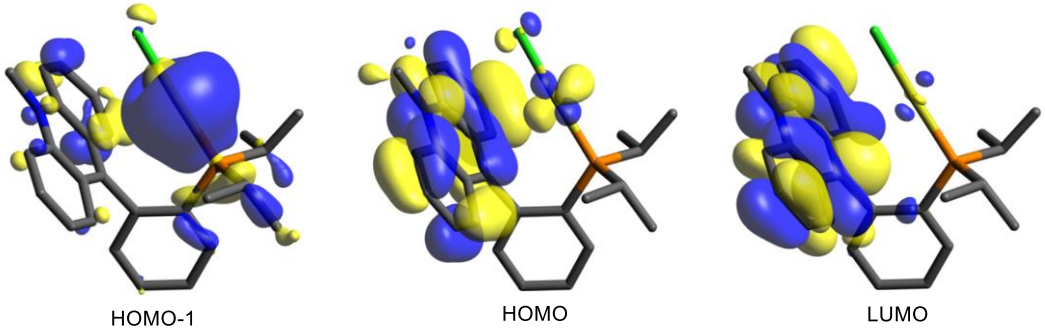

Figure S30. Selected Kohn-Sham orbitals of [**1b**]$^+$ plotted at an isovalue of 0.05.

Table S4. Relevant vertical excitations for $[\mathbf{2a_{in}}]^+$ calculated by TD-DFT

Excited State	Wavelength(nm)	Osc. Strength, f	Major and minor contributions
1	426.1	0.013	HOMO-3 ⟶ LUMO (54%), HOMO-2 ⟶ LUMO (35%)
2	422.5	0.086	HOMO-1 ⟶ LUMO+1 (90%), HOMO-3 ⟶ LUMO (3%)

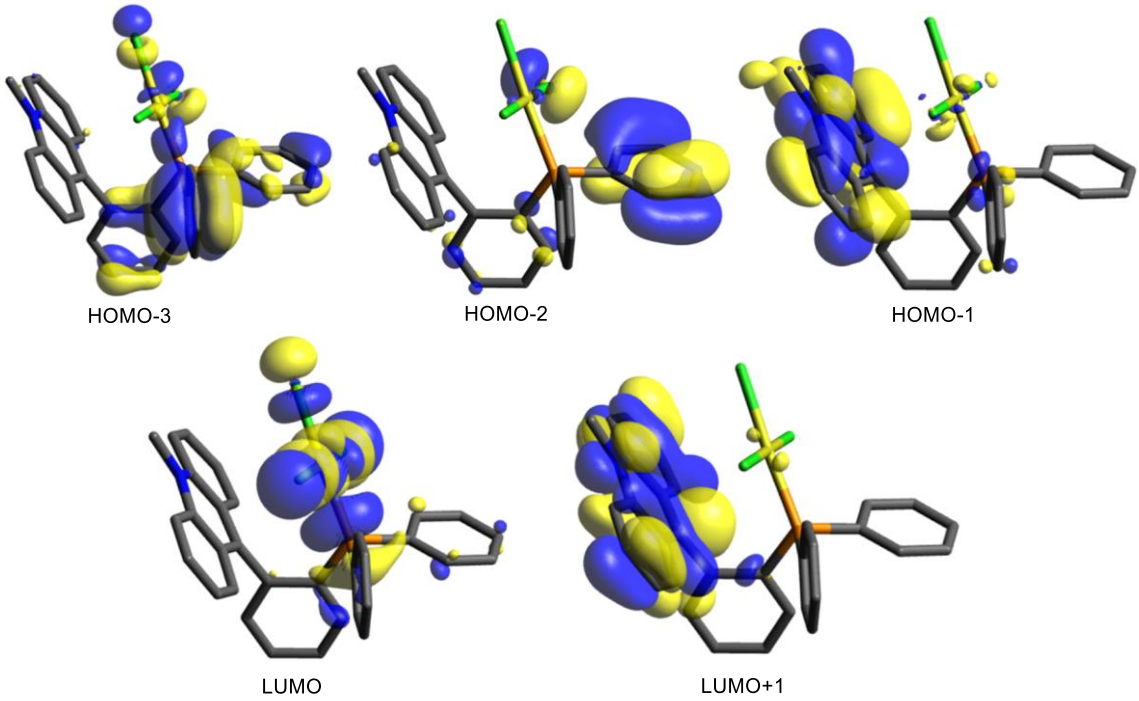

Figure S31. Selected Kohn-Sham orbitals of $[\mathbf{2a_{in}}]^+$ plotted at an isovalue of 0.05.

Table S5. Relevant vertical excitations for $[\mathbf{2b_{in}}]^+$ calculated by TD-DFT

Excited State	Wavelength(nm)	Osc. Strength, f	Major and minor contributions
1	434.5	0.0175	HOMO ⟶ LUMO (74%), HOMO ⟶ LUMO+1 (23%)
2	420.1	0.0419	HOMO ⟶ LUMO+1 (73%), HOMO ⟶ LUMO (24%)

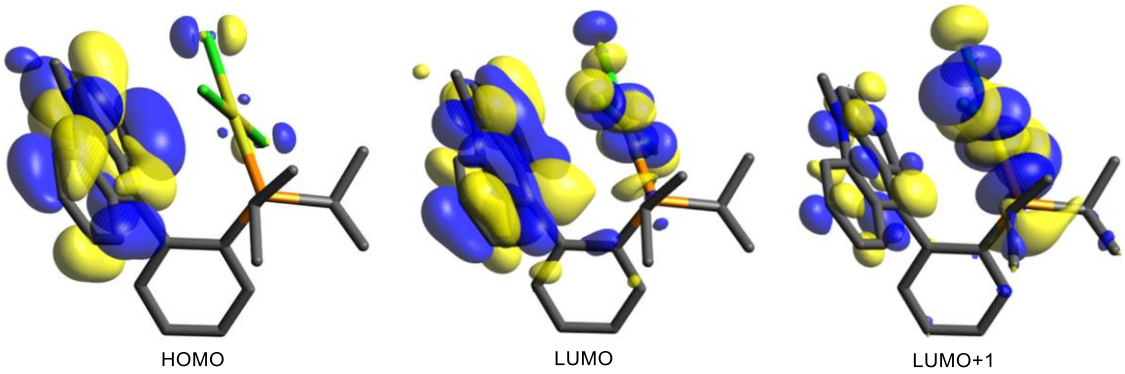

Figure S32. Selected Kohn-Sham orbitals of $[\mathbf{2b_{in}}]^+$ plotted at an isovalue of 0.05.

8.4 Optimized geometries

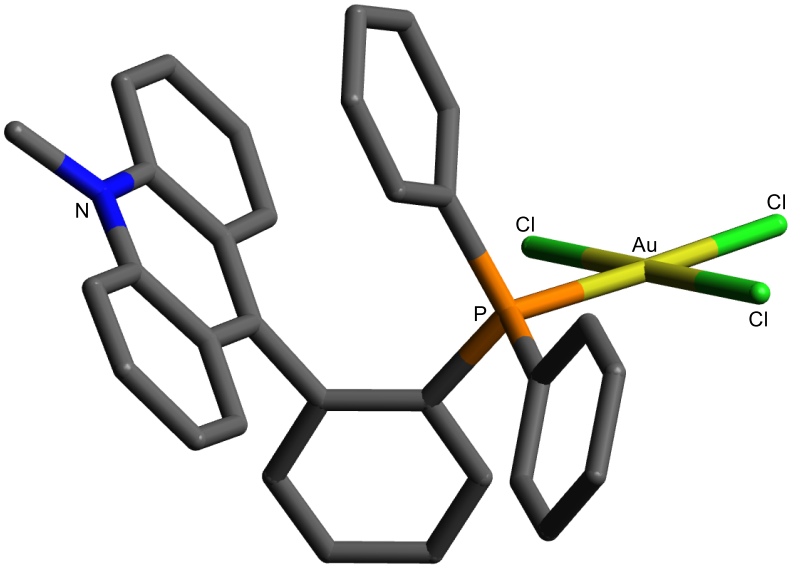

Figure S33. Optimized structure of $[\mathbf{2a_{out}}]^+$

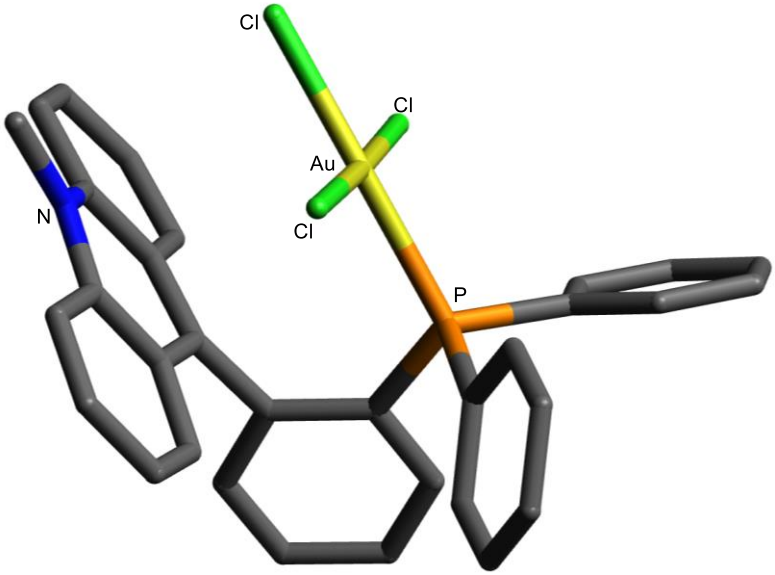

Figure S34. Optimized structure of $[\mathbf{2a_{in}}]^+$

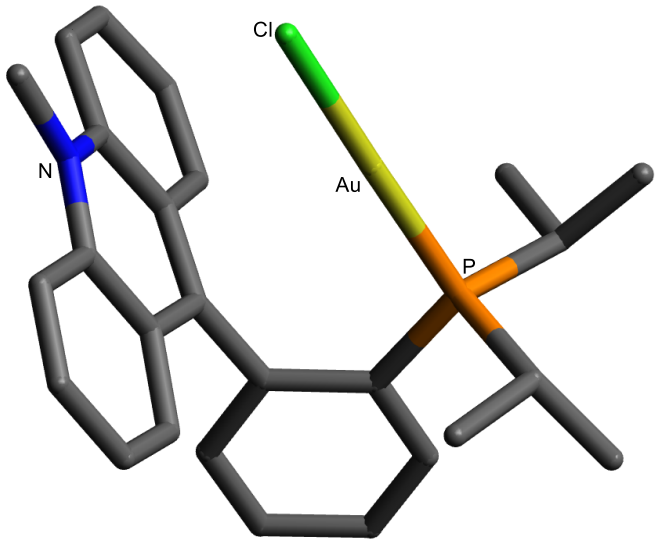

Figure S35. Optimized structure of [**1b**]$^{+}$

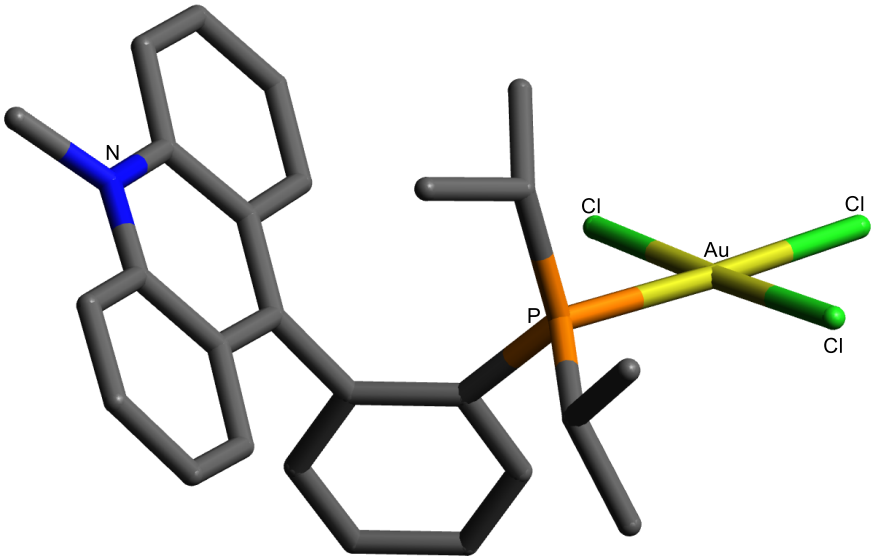

Figure S36. Optimized structure of [**2b**$_{out}$]$^{+}$

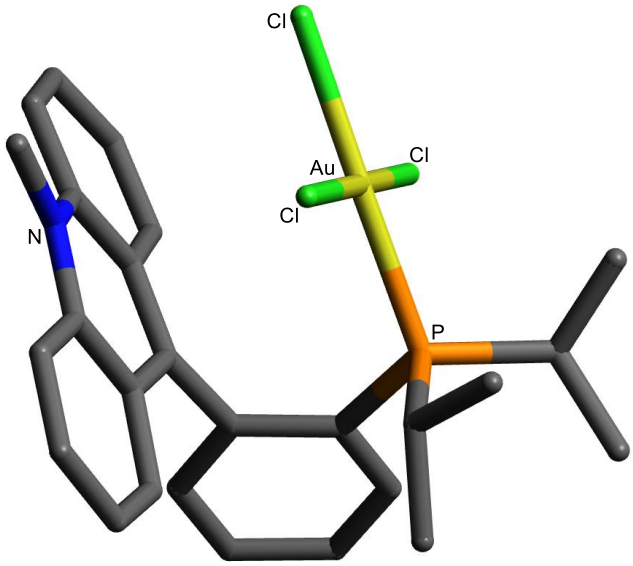

Figure S37. Optimized structure of [**2b**$_{in}$]$^{+}$

8.5 Cartesian coordinates of the geometry optimized structures

Table S6. Cartesian coordinates of the optimized structure of [**1b**]$^{+}$

Atoms	X	Y	Z		Atoms	X	Y	Z
Au	0.04244	-1.41026	-0.55602		H	2.907842	-1.15721	-2.20705
Cl	-1.92767	-2.50591	-0.97632		C	-1.46364	-0.2155	3.849201
P	2.013457	-0.36761	-0.1871		H	-1.0133	-0.38409	4.821956
C	-0.79962	2.627163	-1.5604		C	4.376396	0.327693	-1.70226
H	0.188891	3.030168	-1.37223		H	4.447166	1.371903	-1.38077
C	-1.48297	2.960423	-2.69802		H	4.836757	0.267087	-2.695
H	-1.04034	3.626012	-3.43187		H	4.981313	-0.28892	-1.02952
C	-2.78114	2.443331	-2.90583		C	-3.36655	-0.49113	2.362067
H	-3.33375	2.723202	-3.79783		H	-4.37739	-0.84569	2.211049
C	-3.37209	1.602015	-1.9931		C	0.708282	3.237311	1.459174
H	-4.38103	1.257053	-2.17628		H	-0.231	3.749542	1.650604
C	-2.68499	1.239078	-0.81147		C	0.680922	1.966041	0.868315
N	-3.25134	0.403853	0.111635		C	1.894807	1.289023	0.615549
C	-2.68228	0.205428	1.339859		C	3.091242	1.916875	0.999914
C	-1.36903	0.70997	1.603415		H	4.037078	1.408808	0.843854
C	-0.68579	1.423535	0.597606		C	3.106718	3.176289	1.589431
C	-1.37394	1.767005	-0.58276		H	4.052055	3.629211	1.872775
C	3.137152	-1.35499	0.915712		C	1.907927	3.844659	1.813485
H	4.077119	-0.79546	1.007678		H	1.900475	4.829441	2.270974
C	2.524199	-1.51362	2.307765		C	-0.78501	0.470474	2.879206
H	2.365234	-0.54837	2.799564		H	0.207073	0.861782	3.072776
H	3.199676	-2.10041	2.940234		C	-2.76732	-0.69031	3.583031
H	1.565565	-2.04293	2.261196		H	-3.31636	-1.21495	4.3593
C	3.434195	-2.71548	0.278603		C	-4.47931	-0.32136	-0.23487
H	2.51516	-3.29398	0.129324		H	-4.47342	-1.28552	0.267537
H	4.086632	-3.29268	0.94318		H	-4.4746	-0.536	-1.30087
H	3.944129	-2.62993	-0.68622		H	-5.36619	0.258058	0.040602
C	2.923203	-0.1362	-1.80092		C	2.122174	0.756244	-2.74984
H	2.592138	0.753373	-3.73956		H	1.089476	0.411455	-2.86748
H	2.107656	1.793659	-2.39677					

Table S7. Cartesian coordinates of the optimized structure of $[\mathbf{2a_{in}}]^+$

Atoms	X	Y	Z		Atoms	X	Y	Z
Cl	-1.97008	-1.4591	-2.53592		H	4.085305	0.239382	-1.41158
P	1.593135	0.026653	0.124492		H	3.215378	-0.26068	2.42025
N	-3.66835	0.644493	0.007102		H	6.087432	-3.43372	-0.49164
C	-1.40607	0.349667	1.621698		H	3.399484	4.481669	1.335521
C	-0.34095	0.197499	3.820687		H	2.158159	1.436493	-2.37812
C	-3.45404	-0.55591	0.628316		H	2.291669	-2.59002	1.311792
C	2.563879	2.574184	0.810702		H	3.180921	3.615711	-2.86966
C	-4.66876	0.723559	-1.06399		H	-0.80189	4.897085	1.217592
C	-2.93854	1.754957	0.32635		H	-4.22539	3.176171	-0.70147
C	2.016428	-0.09438	4.183393		H	-0.12437	2.679993	2.059264
C	3.041054	-1.07067	-0.03717		H	-2.87571	5.116506	-0.14537
C	4.194591	-3.13153	0.49031		Au	-0.19925	-0.67755	-1.25171
C	5.184513	-1.56115	-1.04891		Cl	0.123727	-2.80568	-0.44581
C	2.213874	1.702911	-0.22857		Cl	-0.61266	1.427912	-2.08347
C	3.353337	4.191296	-0.79901		H	5.99588	-1.27009	-1.70924
C	0.733603	0.066505	4.69407		H	3.796372	5.157876	-1.02106
C	-2.95862	-3.02604	1.887741		H	0.563642	0.089351	5.766352
C	-4.11504	-2.8281	1.100827		C	-0.16354	0.176422	2.431005
C	1.138088	0.007829	1.907654		C	-2.06638	-2.0029	2.049142
C	4.096154	-0.70887	-0.88568		C	-1.38598	4.015105	0.976589
C	2.209856	-0.12611	2.806382		C	-3.31766	3.03825	-0.12849
C	5.23569	-2.77194	-0.36406		C	-1.00506	2.785046	1.436798
C	3.128341	3.814283	0.522496		C	-2.55797	4.136017	0.196726
C	2.438099	2.089939	-1.5581		C	-4.35811	-1.62955	0.47388
C	-2.29252	-0.73119	1.448731		H	-2.78013	-3.98868	2.355019
C	3.097615	-2.29345	0.650877		H	-1.1716	-2.14308	2.643655
C	-1.76757	1.620807	1.139213		H	-4.8303	-3.63705	0.986027
C	3.01122	3.326415	-1.83689		H	-5.26346	-1.51172	-0.10689
H	-5.6576	0.970575	-0.66528		H	-1.34492	0.323184	4.217017
H	-4.35108	1.472078	-1.78705		H	2.412211	2.288764	1.846872
H	2.868001	-0.1989	4.848777		H	-4.69006	-0.22895	-1.59032
H	4.230675	-4.07313	1.030038					

Table S8. Cartesian coordinates of the optimized structure of $[\mathbf{2b_{in}}]^+$

Atoms	X	Y	Z		Atoms	X	Y	Z
Au	1.10407	3.75043	20.56747		C	3.28611	5.72326	23.97954
P	1.02488	4.44306	18.35851		H	3.67329	5.46003	24.80616
Cl	3.25246	3.13547	20.08538		C	4.04527	5.60543	22.79292
Cl	-1.02785	4.41673	21.05345		H	4.92253	5.24297	22.82449
Cl	1.32231	2.97375	22.75634		C	-0.70726	6.9621	23.8836
N	0.17568	7.15175	22.70627		H	-0.5101	6.09937	24.30435
C	1.43927	6.63946	22.74165		H	-1.64404	6.97854	23.59561
C	1.62821	6.99548	20.33152		H	-0.55132	7.6834	24.52845
C	2.22881	5.79787	18.13816		C	-0.11071	8.34857	19.21475
C	2.36382	6.88364	19.03337		H	0.34607	8.27267	18.38519
C	0.41545	7.69397	20.3699		C	-0.62735	5.10418	17.88962
C	2.01193	6.20577	23.96485		H	-0.90789	5.72068	18.62513
H	1.50921	6.25146	24.76986		C	-1.51018	8.54114	21.63687
C	-0.31234	7.7848	21.5943		H	-2.00755	8.60038	22.44389
C	2.20173	6.54823	21.53494		C	1.15272	3.14797	15.81437
C	3.89582	7.96927	17.49777		H	0.18269	3.05603	15.71184
H	4.43417	8.7177	17.26878		H	1.60352	2.447	15.29784
C	3.80233	6.8843	16.64393		H	1.43456	4.02717	15.48651
H	4.29616	6.87785	15.83254		C	-1.25629	9.07963	19.28551
C	2.9908	5.80652	16.96562		H	-1.59076	9.51793	18.51165
H	2.95276	5.06024	16.37911		C	-0.5948	5.94443	16.59926
C	3.19041	7.94839	18.69519		H	0.17776	6.54687	16.62103
H	3.27584	8.6788	19.29651		H	-1.41831	6.47161	16.53189
C	1.52723	3.01019	17.2999		H	-0.52355	5.3496	15.82367
H	2.5243	2.95179	17.344		C	-1.69417	4.00445	17.80807
C	3.5181	6.01213	21.60209		H	-1.55236	3.47128	16.99812
H	4.03528	5.93664	20.80905		H	-2.58384	4.41411	17.77797
C	0.97655	1.68344	17.85424		H	-1.62736	3.4257	18.59605
H	1.29436	1.55603	18.77233		C	-1.94746	9.1843	20.51411
H	1.28752	0.94144	17.29472		H	-2.73445	9.71451	20.56019
H	-0.00332	1.70849	17.84828					

Table S9. Cartesian coordinates of the optimized structure of $[\mathbf{2a_{out}}]^+$

Atoms	X	Y	Z		Atoms	X	Y	Z
Au	2.789443	-0.60173	-0.14679		H	2.047995	0.680825	2.407661
Cl	4.744321	-1.80323	-0.27793		C	-1.30355	0.835191	-1.93772
Cl	1.755817	-2.41296	0.867608		H	-1.41093	1.854404	-1.58008
Cl	3.826624	1.173814	-1.14184		C	-2.70108	-1.53055	0.656989
P	0.738993	0.569707	-0.02612		C	0.829784	2.373818	-0.23244
C	0.679256	0.362808	4.018689		N	-4.74163	-0.73204	-0.38047
H	1.445101	0.491231	4.777147		C	-1.59128	-0.10908	3.385957
C	-1.26795	0.011406	2.026263		H	-2.61359	-0.35148	3.663899
C	1.212557	4.265709	-1.69235		C	-1.84853	-2.62603	0.97369
H	1.432948	4.656639	-2.68111		H	-0.95531	-2.43743	1.558614
C	0.793278	4.624626	0.656402		C	-3.81213	3.201631	0.745963
H	0.682583	5.295973	1.503056		H	-3.59112	4.22111	1.044176
C	0.05751	0.311822	1.659649		C	-2.08913	0.393638	-2.99828
C	1.056183	5.133654	-0.61259		H	-2.80178	1.073876	-3.45659
H	1.14943	6.205786	-0.75983		C	-1.00143	-1.7596	-2.91632
C	-2.40819	-0.22652	1.093455		H	-0.86563	-2.76383	-3.30667
C	1.109405	2.891993	-1.50709		C	-3.87966	-1.7678	-0.12229
H	1.253403	2.22617	-2.35194		C	-4.43763	0.561213	-0.04031
C	0.680849	3.249959	0.849981		C	-2.12652	-3.88738	0.520976
H	0.49053	2.868716	1.848164		H	-1.46419	-4.71302	0.759163
C	-0.63243	0.067512	4.376429		C	-1.93847	-0.90273	-3.49001
H	-0.91077	-0.03558	5.420841		H	-2.53501	-1.237	-4.33463
C	-0.36076	-0.02474	-1.3537		C	-4.12882	-3.07395	-0.5997
C	-2.99572	2.172096	1.130121		H	-4.97062	-3.2837	-1.24629
H	-2.11516	2.361918	1.732984		C	-5.25331	1.643968	-0.44279
C	-0.21056	-1.32563	-1.856		H	-6.10987	1.490805	-1.08597
H	0.521662	-1.99921	-1.42209		C	-3.26779	-4.10068	-0.28151
C	-3.26778	0.831225	0.738037		H	-3.47363	-5.09506	-0.66725
C	1.014307	0.473976	2.675427		C	-4.93944	2.927828	-0.05813
H	-5.94774	-0.97804	-2.10821		H	-5.57421	3.744704	-0.38891
H	-6.77397	-0.30639	-0.67212		C	-6.02982	-1.02081	-1.01777
H	-6.37132	-2.007	-0.7096					

Table S10. Cartesian coordinates of the optimized structure of [**2b**$_{out}$]$^{+}$

Atoms	X	Y	Z		Atoms	X	Y	Z
Au	2.806855	-0.27929	-0.19387		H	-3.98394	4.291786	0.721819
Cl	4.808256	-1.41015	-0.13583		C	-3.97408	-1.71007	-0.4298
Cl	1.777503	-2.10174	0.791153		C	-4.63035	0.5965	-0.3816
Cl	3.852035	1.473698	-1.23671		C	-2.14909	-3.75039	0.271232
P	0.700156	0.797127	-0.28123		H	-1.4609	-4.54701	0.533674
C	0.427014	0.583467	3.748473		C	-4.16957	-3.03337	-0.88399
H	1.174373	0.718195	4.524061		H	-4.99705	-3.28753	-1.53315
C	-1.44938	0.204343	1.701607		C	-5.48673	1.640129	-0.80351
C	-0.11049	0.480496	1.357788		H	-6.32286	1.446582	-1.46249
C	-2.57323	-0.09003	0.77011		C	-3.27401	-4.02106	-0.53756
C	0.899292	3.249878	-1.77267		H	-3.43909	-5.02966	-0.90535
H	0.232345	2.879583	-2.55551		C	-5.23993	2.937243	-0.4155
C	1.43134	3.370452	0.688386		H	-5.90552	3.723444	-0.75958
H	1.145092	3.081617	1.703074		C	-6.14404	-1.06367	-1.35876
C	-0.89895	0.324197	4.074513		H	-6.0525	-1.04284	-2.44897
H	-1.2153	0.257658	5.110947		H	-6.91762	-0.37003	-1.03678
C	-0.03327	0.211589	-1.89236		H	-6.45145	-2.05463	-1.03038
C	-3.28255	2.275763	0.807065		H	1.931419	3.056466	-2.07027
H	-2.43028	2.50217	1.438653		H	0.763409	4.336205	-1.72252
C	0.076272	-1.28959	-2.15986		H	1.277323	4.45166	0.601005
H	1.098842	-1.66009	-2.05794		H	2.498359	3.174057	0.548802
C	-3.48172	0.923387	0.40758		H	-0.55774	-1.87731	-1.49168
C	0.804391	0.652674	2.414184		H	-0.24687	-1.47955	-3.19009
H	1.852524	0.827423	2.188151		H	-1.48836	0.744867	-3.38008
C	-1.41412	0.744893	-2.28676		H	-2.20408	0.089581	-1.91322
H	-1.61821	1.762935	-1.94354		H	0.709174	0.702097	-2.54139
C	-2.8076	-1.41179	0.349028		H	-0.46813	2.846771	-0.16375
C	0.596091	2.669534	-0.38677		C	-1.91824	-2.4699	0.697222
N	-4.87345	-0.71217	-0.71452		H	-1.03714	-2.2369	1.285512
C	-1.82075	0.132266	3.054412		C	-4.14347	3.264106	0.412325
H	-2.85509	-0.09259	3.301227					

9 X-ray diffraction analysis

9.1 Experimental details

The crystallographic measurements were performed at 110(2) K using a three circle (Quest; Mo Kα radiation, λ = 0.71073 Å) and kappa (Venture; Cu Kα radiation, λ = 1.54178 Å) Bruker-AXS with IμS source and a Photon III area detector diffractometer. In each case, a specimen of suitable size and quality was selected and mounted onto a loop and cooled to 110(2) K in a cold nitrogen stream (OXFORD Crysosystems). The data was collected and reduced using Bruker AXS APEX 3 software[5] and solved by direct methods. Semiempirical absorption corrections were applied using SADABS.[6] Subsequent refinements were carried out using a difference map on F^2 using the SHELXTL/PC package (version 6.1 & OLEX^2).[7] Thermal parameters were refined anisotropically for all non-hydrogen atoms to convergence. H atoms were added at idealized positions and refined using a riding model. The results of these X-ray measurements are provided as CIF files. CCDC 2521156-2521158 contain the supplementary crystallographic data for this paper.

9.2 CCDC deposition numbers

Table S9. CCDC deposition numbers of the crystal structures reported in this work

Compound	CCDC
[**1b**][OTf]	2521156
[**2a**][BF_4]	2521157
[**2b**][OTf]	2521158

10 References

1. L. C. Wilkins, Y. Kim, E. D. Litle and F. P. Gabbaï, *Angew. Chem. Int. Ed.*, 2019, **58**, 18266-18270.
2. G. Park, M. Karimi, W.-C. Liu and F. P. Gabbaï, *Angew. Chem. Int. Ed.*, 2022, **61**, e202206265.
3. M. Roseau, V. De Waele, X. Trivelli, F. X. Cantrelle, M. Penhoat and L. Chausset-Boissarie, *Helv. Chim. Acta*, 2021, **104**, e2100071.
4. N. M. O'Boyle, A. L. Tenderholt and K. M. Langner, *J. Comput. Chem.*, 2008, **29**, 839-845.
5. Bruker, 2019, APEX3 (v2019.2011-2010), Bruker AXS Inc., Madison, Wisconsin, USA.
6. G. M. Sheldrick, *Journal*, 2016.
7. a) G. M. Sheldrick, *Acta Crystallogr. A*, 2015, **71**, 3-8; b) O. V. Dolomanov, L. J. Bourhis, R. J. Gildea, J. A. K. Howard and H. Puschmann, *J. Appl. Crystallogr.*, 2009, **42**, 339-341.